Post-print of: Wójcik M., Sondej M., Rejowski K., Tejchman-Konarzewski A.: Full-scale experiments on wheat flow in steel silo composed of corrugated walls and columns. POWDER TECHNOLOGY. nr. 311 (2017), s. 537-555. DOI: 10.1016/j.powtec.2017.01.066

Full-scale experiments on wheat flow in steel silo composed of Corrugated walls and columns

M. Wójcik, M. Sondej, K. Rejowski, J. Tejchman *

Gdańsk University of Technology, Faculty of Civil and Environmental Engineering, G. Narutowicza 11/12, 80-233 Gdańsk, Poland

a b s t r a c t

The paper describes experimental investigation results on wheat flow in a medium-size steel cylindrical flat bot-tom silo with horizontally corrugated walls and columns composed of open-sectional thin-walled profiles. Sev-eral experiments on silo filling and emptying with wheat were performed by inducing a different flow pattern. The following quantities were measured in the silo: horizontal wall pressures, wall frictional tractions and verti-cal reaction forces under columns. Horizontal wall pressures and wall frictional tractions were registered along the silo height and silo circumference in the lower silo region during three different flow patterns: mass flow, mixed mass-funnel flow and eccentric flow. Experimental results were compared with Eurocode 1. Some dis-crepancies between experiments and code formulae were observed.

Keywords: Experiments, Silo, Corrugated wall, Flow pattern, Wall pressure, Wheat

1. Introduction

Silos are engineering structures widely used in industries and farms to store, feed and process bulk solids that is essential to agricultural, mining, mineral processing, chemical, shipping and other industries [1–7]. They are mainly built from reinforced concrete, steel and aluminium. In spite of extensive experimental and theoretical studies of silo problems, silos fail with a frequency much higher than the rate of structural failure of other industrial structures [8–10]. The failures are connected with large economic loss and accompanying people accidents due to design, construction and user errors. Silo failure can be devastating as it can result in loss of the container, contamination of the material it contains, loss of material, clean-up, replacement costs, environmental damage and possible injury or loss of life. Most of silo failures take place at the onset of discharge and they usually lead to catastrophic collapse of the entire silo. They are mainly caused by a lack of knowledge concerning complex characteristic phenomena occurring in bulk solids in silos in the interaction with the silo structure. Non-symmetric wall pressures, seismic and wind loads, stresses created by temperature difference between the silo wall and stored bulk solids, potential internal explosion of the stored material and differential settlement of the foundation or support columns should be considered during the design process. Characteristic phenomena which may be created during confined flow of granular bulk solids in silos are: e.g. sudden and significant increase of wall stresses, different flow patterns, formation and propagation of both wall and interior shear zones, fluctuation of pressures and strong autogeneous dynamic-acoustic effects [11]. In addition, each silo flow is influenced by the size effect which is mainly due to a different pressure level in silos and also due to a different ratio between the mean grain diameter of the bulk solid and silo diameter/width [11]. Normalized wall pressures (with respect to the silo dimensions) diminish with increasing silo size since the larger pressure decreases both the strength (expressed by mobilized internal friction) and deformability (expressed by dilatancy) of bulk solids. In addition wall pressures reduce with decreasing ratio between the mean grain diameter and silo size due to the presence of shear zones with a defined thickness (related to the mean grain diameter) [11]. In general, the behaviour of bulk solids in silos is similar to the solid shear behaviour along the wall with the different roughness between two states: shearing with free volume changes and shearing with constrained volume changes [12]. A different distribution of bulk solids in small and large silos contributes also to a statistical size effect [12].

Metal silos can be built of thin-walled isotropic plain rolled sheets (which can be welded, riveted or screwed around the silo perimeter) or of thin-walled corrugated curved sheets strengthened by vertical stiffeners (columns) distributed uniformly around the silo circumference and connected with screws. Those latter are frequently used in the engineering practice due to an economical steel consumption (small silo weight) and larger buckling resistance [13,14]. In these silos, horizontally corrugated wall sheets carry circumferential tensile forces caused by horizontal wall pressure and columns carry vertical compressive forces due to the vertical wall friction traction exerted

http://dx.doi.org/10.1016/j.powtec.2017.01.066

from bulk solids. Thin-walled metal cylindrical silo shells are vulnerable to buckling failure caused by the wall friction force due to shearing of bulk solids along silo walls [15,16]. The buckling failures occur particularly during silo eccentric discharge. As a consequence of eccentric emptying, non-uniform horizontal wall pressures develop which contribute to meridional bending and a non-symmetric distribution of wall compressive forces. Even for silos designed for concentric discharge, eccentric discharge effects are difficult to avoid due to material segregation. It is of a mayor importance for the optimum silo dimensioning to know load distributions from the stored material exerted on the silo structure which depend on the flow pattern. In contrast to experiments in cylindrical metal silos composed of thin-walled isotropic plain rolled sheets (e.g. [17–29]), the extensive experimental measurements in cylindrical silos with corrugated walls are lacking. The aim of our research works at Gdansk University of Technology is to elaborate realistic dimensional procedures for buckling of cylindrical metal silos composed of corrugated walls and columns, which are at present frequently used in the engineering practice, based on comprehensive measurements in full-scale silos and FE analyses [30–32]. In the procedures, the effect of the bulk solid will be taken into account [15,16]. Full-scale experiments include measurements of wall pressures and wall frictional tractions during filling and emptying and buckling tests with an empty and a pre-filled silo.

In the first step we carried out several experiments on wall horizontal pressures and wall frictional tractions in a full-scale metal cylindrical silo with corrugated walls and columns (height ≅ 7.5 m, diameter ≅ 2.7 m) during filling and emptying using wheat as a stored material (frequently used in the silo practice). Attention was paid to the distribution of wall horizontal pressures and wall frictional tractions along the silo height and circumference, mobilisation grade of corrugated wall friction and flow pattern occurrence. The silo had 5 circular outlets. Over 25 tests in a model silo containing dry wheat were performed. Three different flow patterns were studied: concentric mass flow, concentric mixed mass-funnel flow and eccentric flow obtained by opening different outlets. In order to separately measure wall loads in a horizontal and vertical direction from the stored bulk solid, novel load cells were developed. In addition, the vertical reaction forces in columns were measured. The experimental results of wall horizontal pressures and wall frictional tractions were compared with Eurocode 1 (EC1) [33]. The difference between

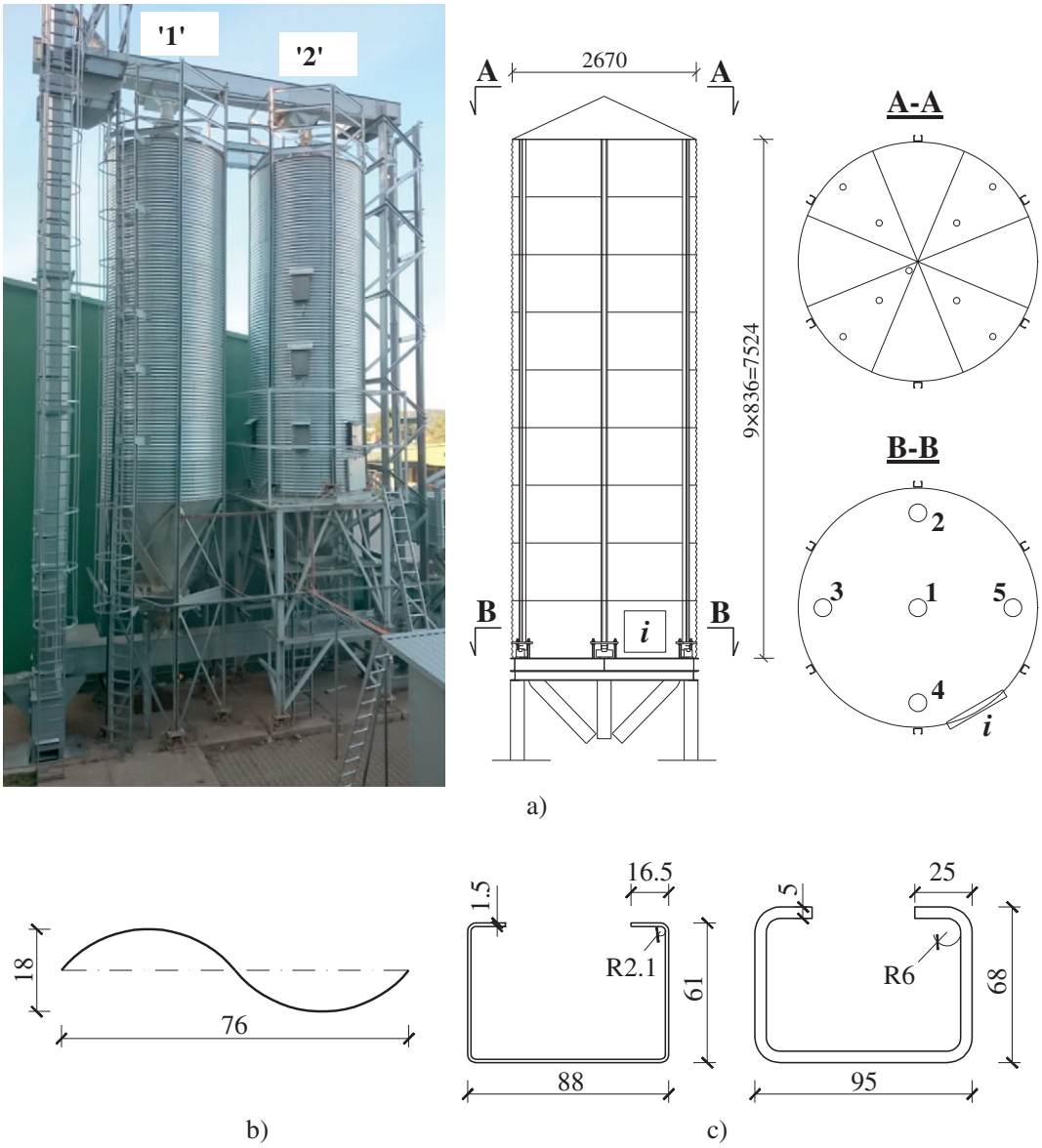

Fig. 1. Experimental set-up: a) measuring silo '2' ('1'–'5' - outlets, *i* - inspection opening door) and storage silo '1', b) wall corrugation and c) column profiles (units are in [mm]).

experimental and EC1 results were outlined. To our knowledge, such comprehensive experiments have not been performed in silos with corrugated walls and columns yet. Our experimental results will create also a solid basis for validating numerical calculation results of wall pressures in silos during flow based on FEM and a micro-polar or non-local hypoplastic constitutive model for non-cohesive and slightly cohesive bulk solids [11,34].

2. Experimental set-up

The experimental mid-size silo station consisted of 2 slender steel cylindrical silos, material transport system and measuring instrumentation which allowed for studying the behaviour of wheat during a filling and emptying process (Fig. 1). One silo (called '1', Fig. 1) was used for a wheat storage and the second one (called '2', Fig. 1) for measurements of wall loads. The silos had the diameter of $D = 2.67$ m. The height of the silo cylindrical part was $H = 7.524$ m ($H/D \approx 3$). The capacity of each silo was approximately 42 m^3 (33 t for wheat). The silos were built of 9 rings which were made of horizontally corrugated sheets (thickness $t = 0.75$ mm). The corrugation height d and width l were $d = 18$ mm and $l = 76$ mm (Fig. 1b). The silos included 6 columns composed of open-sectional thin-walled cold-formed profiles which were at the distance of 1.4 m. The column profiles were of the type 'C' with the thickness t_c varying from 1.5 mm at the top down to 4 mm at the bottom (Fig. 1c). The measuring silo '2' was supported on a steel frame built of 4 hot-rolled beams and 4 braced columns. The roof was conical with the inclination angle to the horizontal of 25°. The measuring silo '2' had a flat bottom with 5 outlets with the diameter of 0.2 m which allowed for bulk solid flow due to gravitation with the mass flow rate up to 160 t/h. For silo filling, two horizontal conveyors (top and bottom screw feeders with the mass flow rate of 150 t/h) and a vertical bucket elevator were used. The storage silo '1' had a conical hopper with a centrally located outlet with the diameter of 0.4 m. By opening various outlets, different flow patterns might be obtained in wheat (concentric mass flow, concentric mixed mass-funnel flow and eccentric flow).

The specially constructed 8 wall load cells (C1–C8) in the corrugated wall and 1 load cell (C9) in the wall inspection opening were used in the silo '2' of Fig. 2 in order to directly measure solid loads on the wall in a horizontal and vertical direction. The direct measuring cell surface was 19×23 cm^2 and was made of a sheet cut out from the silo wall (Fig. 3A). During installation of load cells, the full alignment of load sheets with the silo wall was ensured [35,36]. The gap of 1–2 mm between the measuring sheet surface and silo wall silo was filled with a plastic paste. The measuring sheet was fixed to two standard bending beam load cells (produced by the ZEMIC company) which were connected together in a L-shaped configuration. The beams were closed in the rigid frame (4 C-profiles C80) which was mounted to the silo wall. The load cell had the stiffness of 0.550 kN/mm in the horizontal

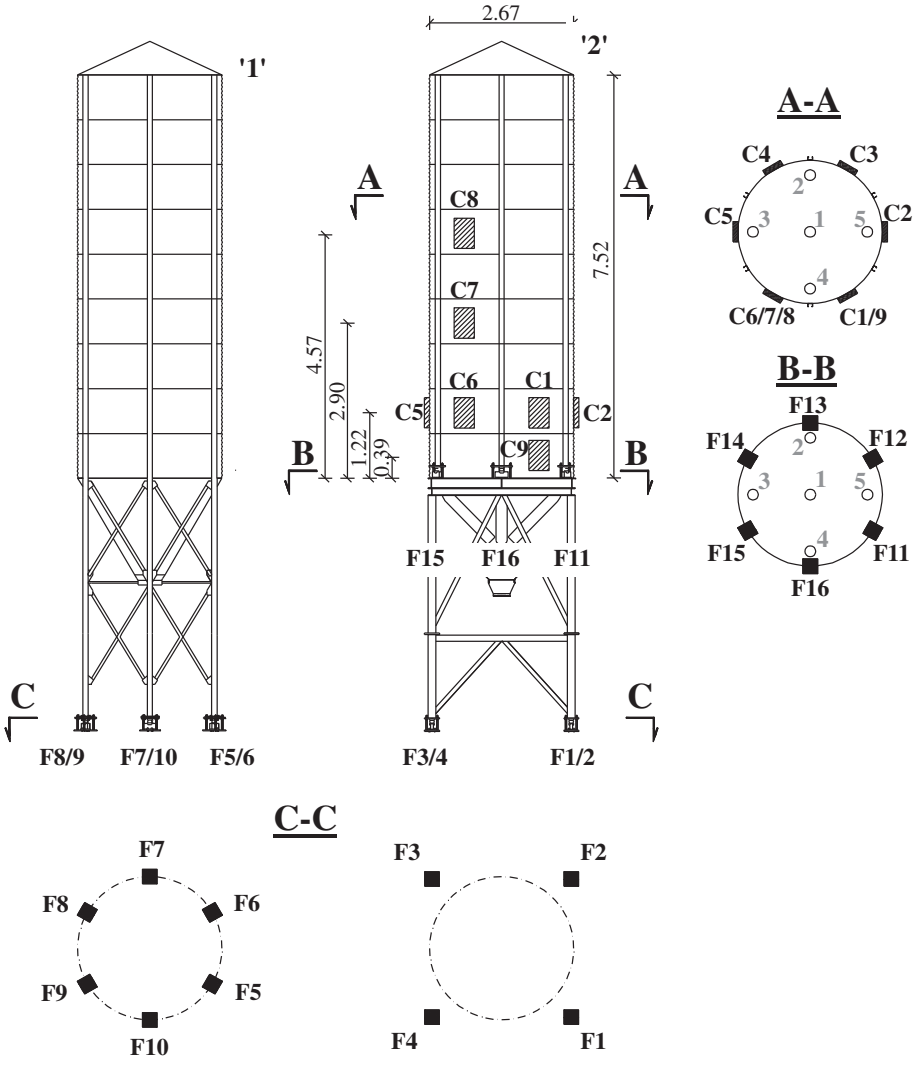

Fig. 2. Cylindrical metal silos (storage silo '1' and measuring silo '2') used in experiments (diameter $D = 2.67$ m): location of load cells C1–C9 in corrugated wall and vertical reaction force transducers F1–F16 under silo columns and supporting frame columns

direction and 2 kN/mm in the vertical direction. Each load cell had its outer cover against the influence of weather conditions. The load cells were able to register the wall load both in a horizontal and vertical direction independently from each other. The contact area of the measuring surface included 3 folds of the corrugated wall. The load cells were calibrated at the laboratory of Gdansk University of Technology by applying loads in a normal and tangential direction within the expected silo load range. Note that the measuring surface in the cell '9' (located in the inspection opening door at the silo bottom) was flat. In order to measure vertical reaction forces in silo columns, 16 load cells (manufactured by KELI SENSING TECHNOLOGY) were used (Fig. 3B) in the load range of 0–200 kN: 4 under the frame supporting the flat-bottomed silo (denoted as '1'–'4'), 6 in the silo with the conical hopper ('5'–'10') and 6 under the flat-bottomed silo ('11'–'16'). The cells were equipped with a ball-joint (protected by a rubber membrane) and was resistant to weather conditions. The data acquisition system included a 40-channel measuring device produced by the APEK company which recorded measurements at the frequency of 2 Hz.

The silo was always pre-filled in an usual industrial way, i.e. the solid was transported to the silo top with the aid of a bucket elevator and screw feeder and then poured in inside the silo with the aid of an inlet opening situated in the mid-roof. After filling, the top surface had a shape of a conical heap located about 0.5 m below the roof. Based on the material weight and silo geometry, the mean initial specific weight of wheat was $\gamma = 7.75 \pm 0.1$ kN/m^3. The repose angle of wheat based on the inclination of the wheat conical top boundary in the silo was $\phi = 24°$. It was similar as the angle determined at the laboratory with the aid of a fixed funnel method. The wheat grain diameters changed between 1.5–6 mm (the mean grain diameter was $d_{50} = 1.9$ mm) based on a usual sieve analysis.

The wheat flow type was approximately determined by means of special markers that moved with the material. The spherical markers with many protrusions had the diameter of 3 cm and were placed in wheat at different heights in two perpendicular planes along the silo diameter. They were put from the silo roof during silo filling with the aid of a steel tube with the diameter of 3.5 cm. The markers were dropped during filling when the tube's end touched the bulk solid. The tube was then gradually pulled up to the next level. This procedure was repeated until the silo was completely filled. During emptying, the numbered markers after moving through the outlet equipped with a steel sieve were collected and their residence time was noted. The surface profile during discharge was measured every five minutes at nine positions of markers. It was achieved with the help of measuring tapes loaded at their ends and lowered through roof openings (the use of laser rangefinders was impossible due to a high dust concentrations inside the silo).

3. Wall loads according to Eurocode 1

3.1. Wall loads for concentric filling and emptying

The horizontal (normal) pressure p_h and frictional traction (called shear pressure) p_w along walls during concentric silo filling and emptying were calculated according to Eurocode 1 [33] (following strictly the slice-method by Janssen):

$$p_{hf}(z) = \frac{\gamma \cdot A}{\mu_{eff} \cdot U} \cdot Y_J(z), \quad p_{he}(z) = C_h \cdot p_{hf}(z) \tag{1}$$

and

$$p_{wf}(z) = \mu_{eff} \cdot p_{hf}(z), \quad p_{we}(z) = C_w \cdot p_{wf}(z) \tag{2}$$

with

$$Y_J(z) = 1 - e^{(-z \cdot K \cdot \mu_{eff} \cdot U/A)} \tag{3}$$

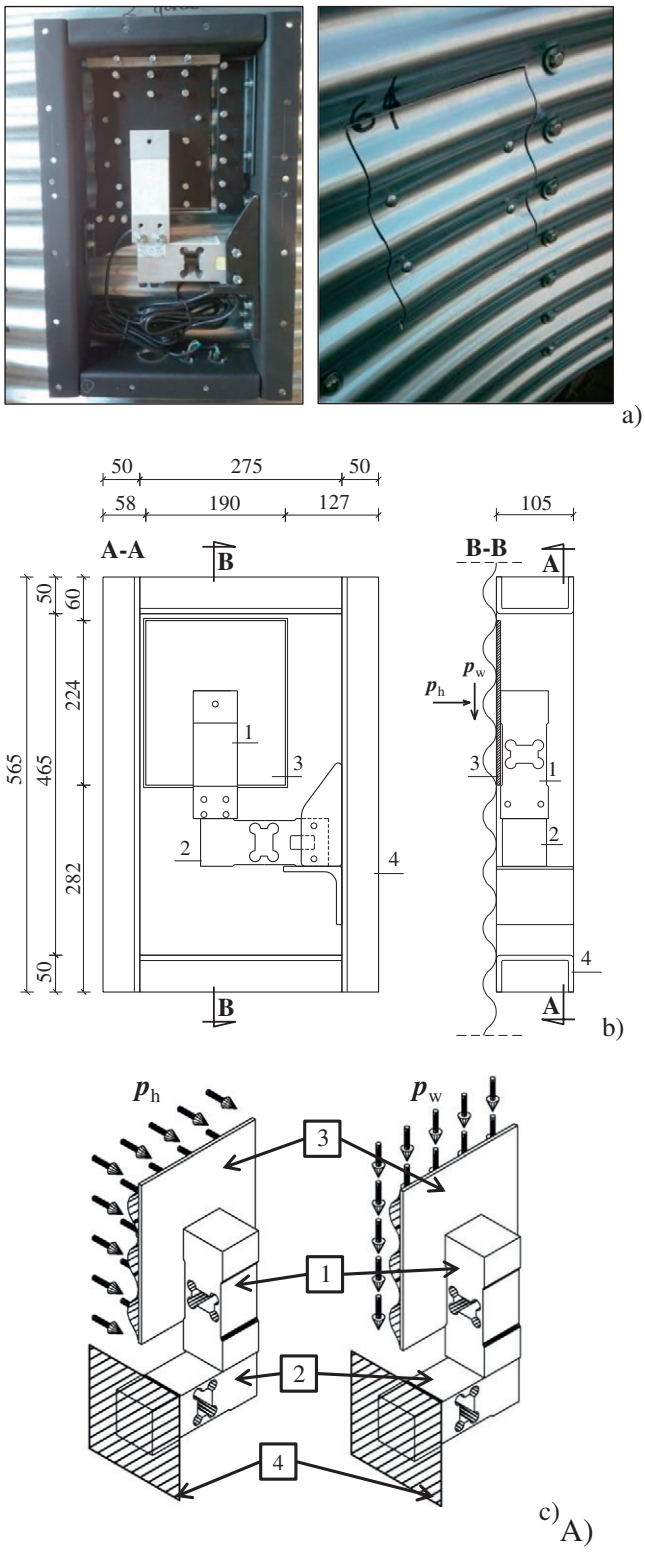

Fig. 3. Load cells used in silos '1' and '2': A) wall load cell: a) view on uncovered and covered cell from silo inside, b) construction and c) measurement principle (1 - normal wall pressure measuring beam, 2 - tangential wall pressure measuring beam, 3 - measuring surface, 4 - external frame, p_h - horizontal wall pressure, p_w - frictional wall traction and B) view on support load cell: a) located under supporting frame columns, b) located under silo columns and c) construction (1 - load cell, 2 - column profile, 3 - screw, dimensions are in [mm])

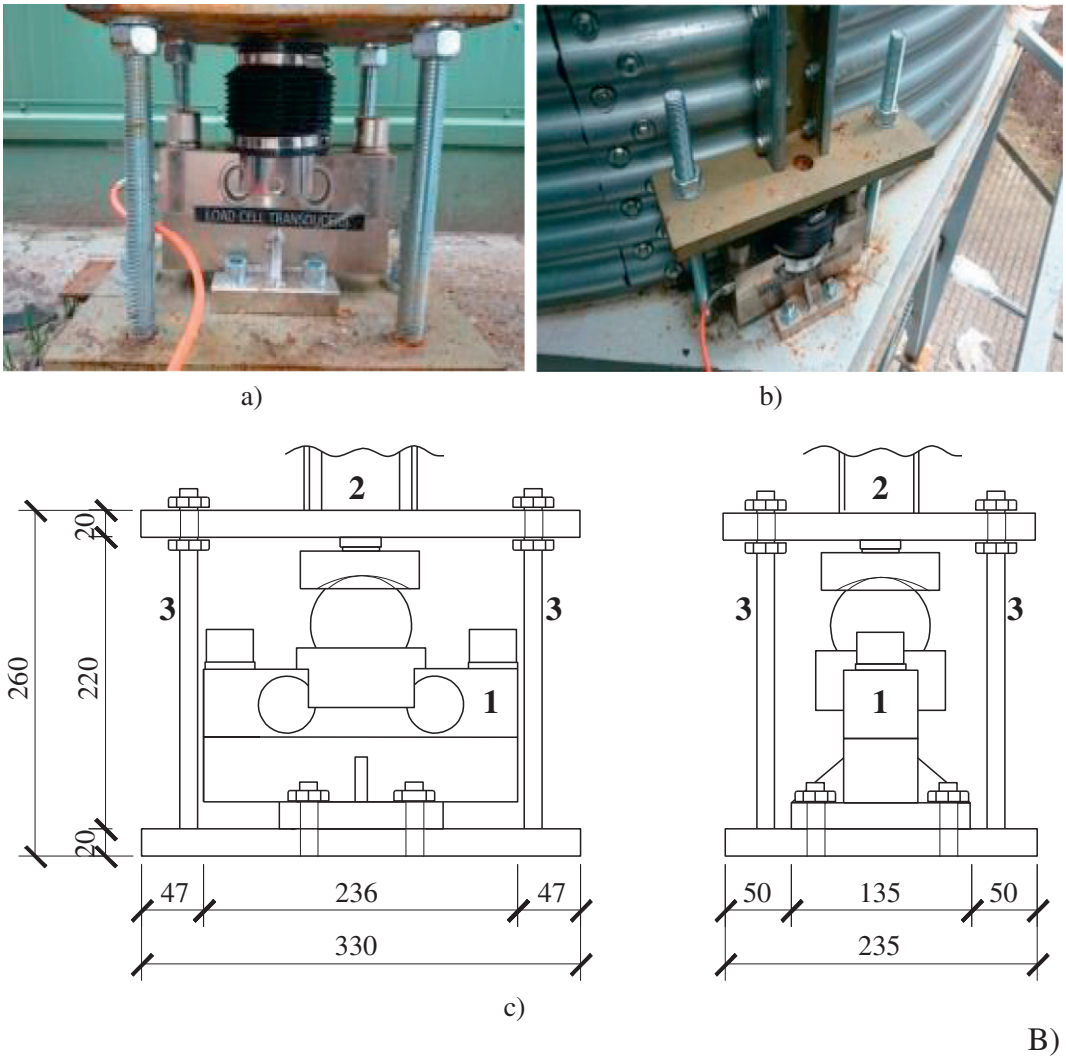

Fig. 3 (*continued*).

where γ is the solid volumetric weight, K - the horizontal-to-vertical pressure ratio, z - the depth under the equivalent material surface, A - the cross-section area and U - the internal circumference, C_h and C_w – the horizontal and frictional emptying factors (the subscript 'f' denotes filing and 'e' emptying). The effective wall friction coefficient μ_{eff} between the fill and corrugated wall is

$$\mu_{eff} = (1-a_w) \cdot \tan\varphi_i + a_w \cdot \mu_w \quad (4)$$

where a_w - the wall contact factor, μ_w - the wall friction coefficient between the solid and flat sheet and ϕ_i - the residual internal friction angle of wheat.

In order to show differences between theoretical (standard) and measuring outcomes, the theoretical wall loads were determined for the mean characteristic values of wheat in the silo of the Reliability Class 1 according to EC1: $a_w = 0.2$, $\mu_w = 0.38$, $\phi_i = 30°$ (residual internal friction angle of wheat), $\phi_r = 34°$ (angle of repose), $\mu_{eff} = 0.54$ ($\varphi_w = \arctan(\mu_{eff}) = 28°$ – corrugated wall friction angle) (Eq. (4)), $\gamma = 8.25$ kN/m^3, $K = 0.54$ (pressure ratio), $C_h = 1.9$ and $C_w = 1.4$ (with the outlet eccentricity $e = 0$ m and local pressure coefficient $C_{op} = 0.5$). In general the standard range of μ_{eff} for wheat may be 0.47–0.62 (mean value - 0.54). The standard maximum horizontal wall pressures were: $p_{hf} = 9.8$ kPa and $p_{wf} = 5.3$ kPa during silo filling and: $p_{he} = 18.6$ kPa and $p_{we} = 7.4$ kPa during emptying. The distribution of p_h and p_w is shown in Fig. 4. The maximum vertical compressive force in a single column was calculated as $N_f = 39.3$ kN (filling) and $N_e = 55.1$ kN (emptying).

According to EC1, in order to take asymmetric behaviour of the bulk material into account, an additional asymmetric normal wall pressure located at a certain silo height (so called "patch load") is taken into account. For our silo this additional wall pressure was 10% for filling and 20% for emptying of the total one. It may be, however, ignored for our research silo since it belongs to the Reliability Class 1.

3.2. Wall loads for eccentric outflow

During experiments, a flow channel geometry could not be measured. Therefore the calculations for eccentric outflow were performed for 3 different flow channel radii r_c of Fig. 5 following EC1

$$r_c = 0.25R, \quad r_c = 0.4R \quad \text{and} \quad r_c = 0.6R, \quad (5)$$

where: $R = D/2$ is the silo radius.

The flow channel wall contact angles θ_c and ψ are defined as

$$\theta_c = \cos^{-1}\left(\frac{R^2 + e_c^2 - r_c^2}{2Re_c}\right) \quad (6)$$

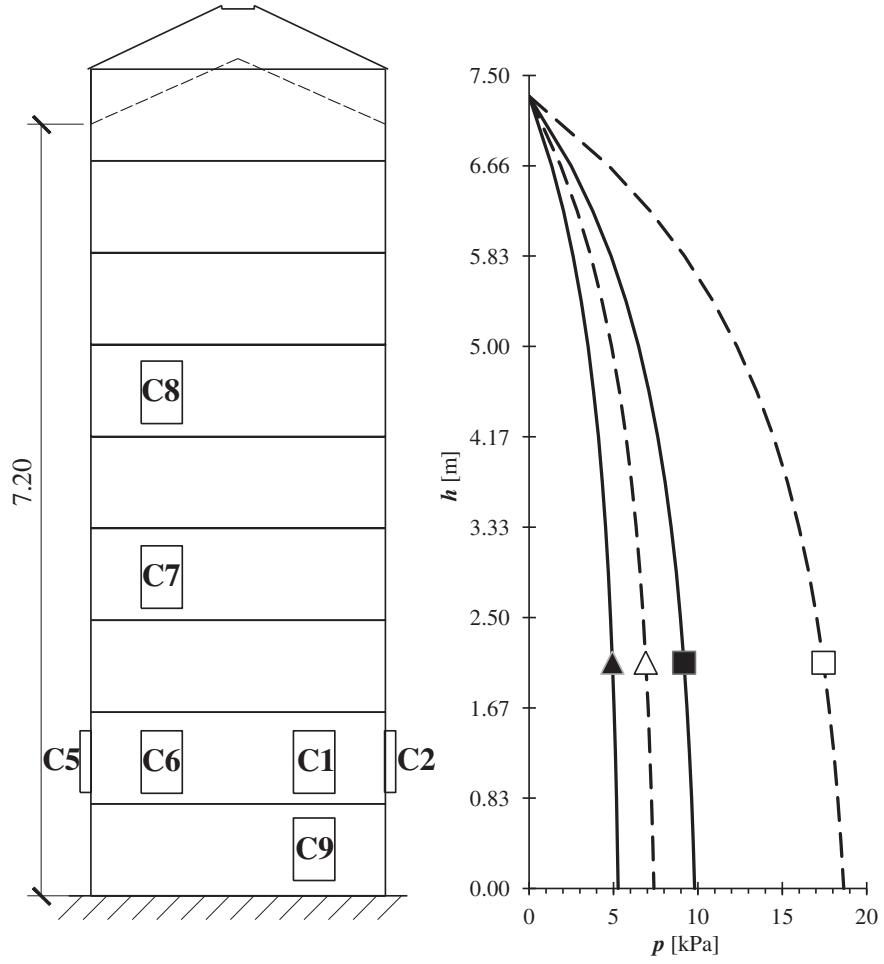

Fig. 4. Horizontal wall pressures and wall frictional traction p [kPa] in experimental silo during symmetric filling and emptying according to EC1 (▲ - frictional traction for filling p_{wf}, Δ - frictional traction for emptying p_{we}, ■ - horizontal pressure for filling p_{hf}, □ - horizontal pressure for emptying p_{he}, C1, C2, C5–C9 - load cells)

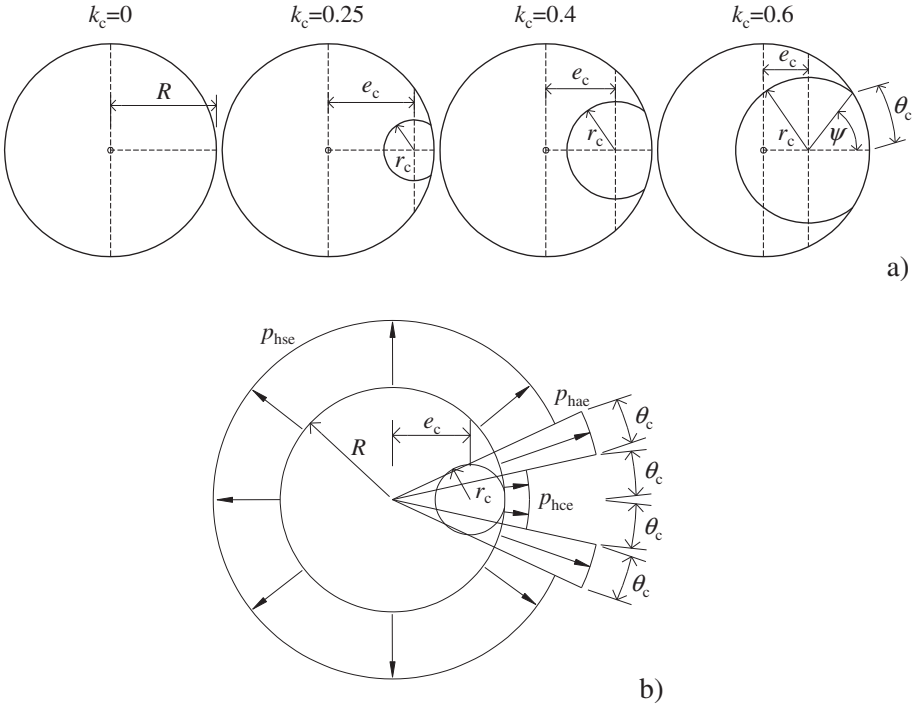

Fig. 5. Eccentric emptying by EC1: a) geometry of 4 different discharge conditions (independent of silo aspect ratio), b) pressure distribution (e_c - flow eccentricity, r_c - flow channel radius, θ_c and ψ - flow channel angles, R - silo radius and k_c - r_c/R)

and

$$\psi = \sin^{-1}\left(\frac{R}{r_c}\,\sin\theta_c\right). \tag{7}$$

The calculated horizontal wall pressure distribution on the vertical wall in the flowing zone for 3 values of r_c (Eq. (5)) is demonstrated in Fig. 6. The highest wall pressures occurred for the lowest flow channel radius ($r_c = 0.25R$). The wall pressure close to the flow channel was significantly reduced ($p_{hce} = 2.4$ kPa) whereas at the flow channel edge, the horizontal wall pressure was the highest ($p_{hae} = 16.6$ kPa), i.e. higher by 75% than during filling. The horizontal wall pressure far beyond the flowing channel in the zone (where the solid remained motionless) was the same as during filling ($p_{hse} = p_{hf} = 9.5$ kPa).

4. Experimental results

4.1. Wheat flow with one centrally open outlet '1'

Fig. 7a shows the surface profiles of wheat observed from the silo top and Fig. 7b presents the emptying times for markers located at different silo levels for one cross-section (discharge flow rate was 65 t/h) for one arbitrary test. When the outlet was opened, the material started to flow and the upper boundary of wheat moved slowly down along the wall. Later the flowing channel diameter observed from the top became smaller until the surface profile reached a dip shape and wheat started to slide down along the corrugated wall. Thus, the markers in the mid-region (lines 'H', 'I' and 'F' in Fig. 7b) came out first in a mass flow order but markers located adjacent to the walls came out down in a reverse sequence, i.e. the markers located at higher levels came out before those at lower levels, implying that wheat remained stagnant close to the wall until the markers were collected. The markers located close to the silo wall and near the silo bottom came out at the latest. The average flowing channel diameter was between 1.2 m and 2.4 m (Fig. 7b). This mixed mass-funnel flow profile was slightly non-symmetric (Fig. 7). The height of the mass flow zone in the upper silo region was about 2 m and the funnel flow happened from the outlet height up to about $H = 5.5$ m (based on the observations of the top surface (level III in Fig. 7).

The evolution of horizontal (normal) and shear wall pressures and mobilized wall friction coefficient/angle on the corrugated silo wall for the pressure cells located along the silo height (load cells: C6–C8) during silo filling and emptying for one arbitrary tests is presented in Fig. 8 and for the pressure cells located along the circumference at the silo bottom (load cells C1–C6 of Fig. 2) in Fig. 9. The distribution of the horizontal and shear wall pressures (maximum values) during filling and emptying onset is shown in

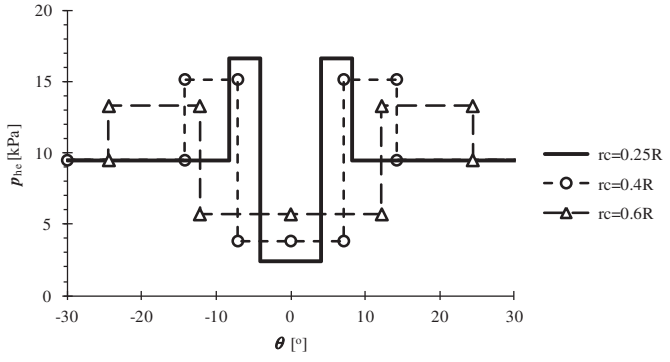

Fig. 6. Calculated distribution of horizontal wall pressure p_{he} along silo circumference in experimental silo at height of cells walls C1–6 of Fig. 2 during eccentric flow according to EC1 (r_c - flow channel radius and θ - angle with respect to silo centre).

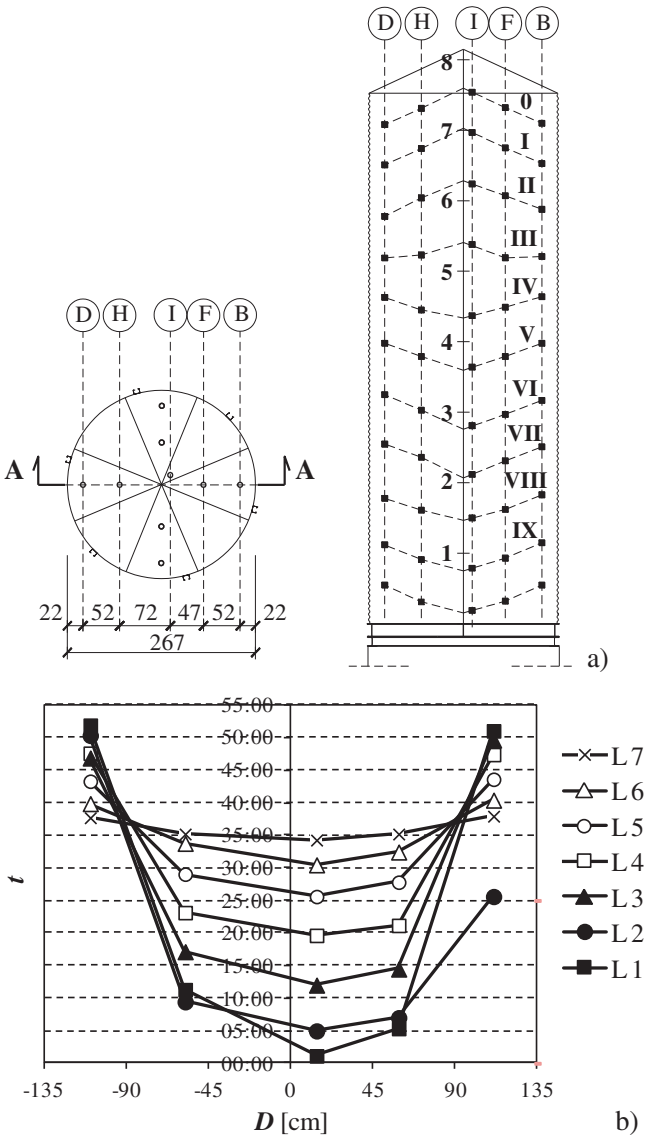

Fig. 7. Experimental results for corrugated silo with one centrally open outlet: a) surface profiles of wheat (0 - filling level, I-X - subsequent emptying stages every ~5 min) and b) emptying times for markers located at different levels in cross-section D-H-I-F-B from one arbitrary test (L1–L7 - initial markers positions starting from silo bottom every 1 m, D - silo diameter and t - emptying time).

Fig. 10a along the silo height and in Fig. 10b along the silo circumference.

During filling, each curve followed a similar non-linear distribution trend as given by the Janssen theory (i.e. the pressure gradient diminished during continuous filling and each curve approached its asymptote) (Fig. 10a). As the solid started to flow, the horizontal and shear wall pressures immediately increased due to shearing along the wall connected with volume changes (except of the highest located cell '8'). Next they remained nearly constant for a short time and then decreased. The wall pressures did not grow solely at the bottom due to funnel flow (load cell 9). The distribution of horizontal wall pressures was rather linear (Fig. 10a) in contrast to the distribution assumed by EC1. The results were found to be repeatable (the coefficient of the stress variation was 9.3%). The largest filling wall pressures appeared at the lower silo part (10.5 kPa for the horizontal wall pressure (C2) and 5.3 kPa for the shear wall pressure (C3) of Fig. 2). The highest increase during emptying also occurred in the lower silo region (pressure cells C1 and C3, located 1.2 m above the silo bottom) in the region close to the effective transition between mass and funnel flow. The horizontal

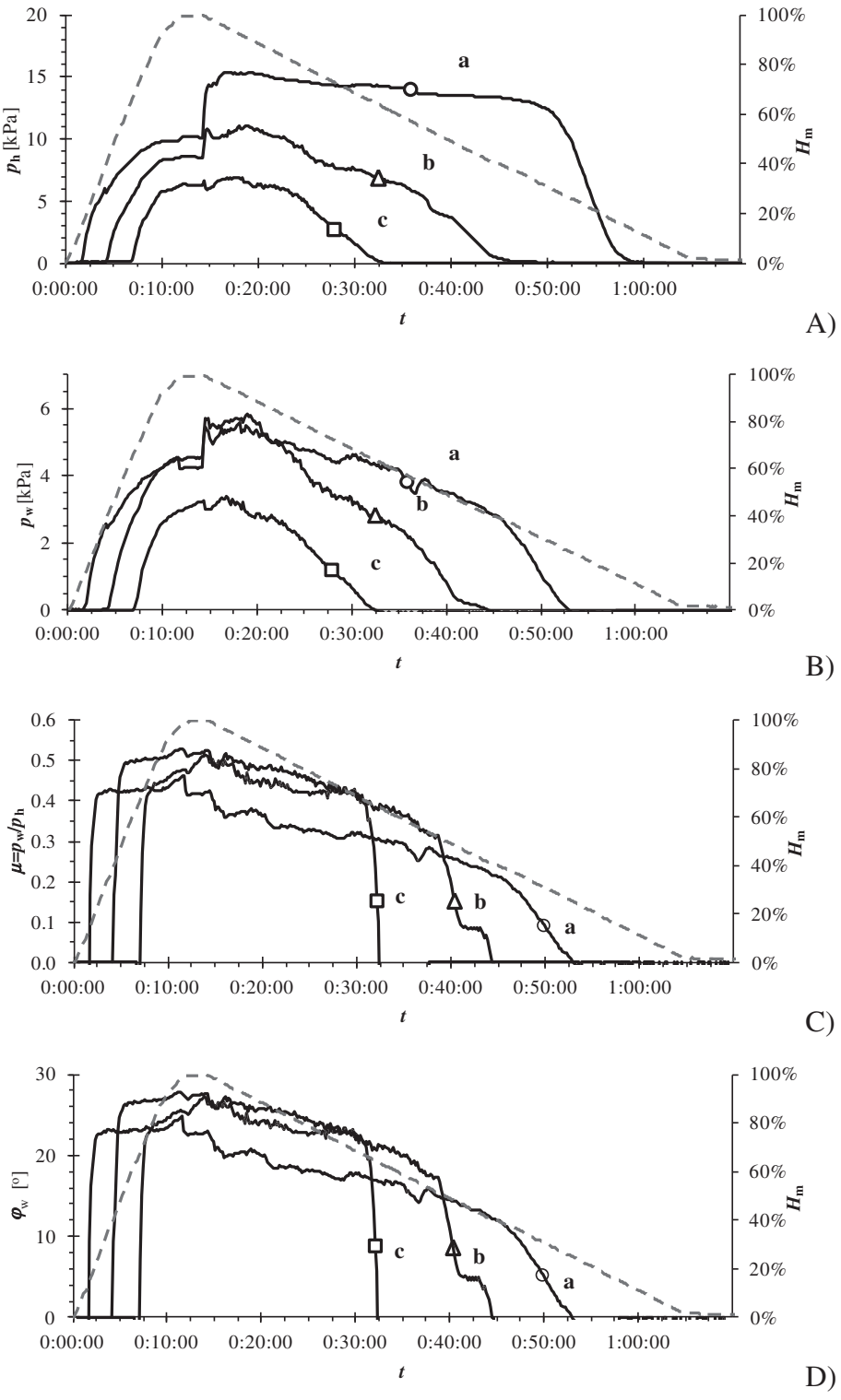

Fig. 8. Measurements from one arbitrary test with one centrally opened outlet: evolution of horizontal wall pressure p_h (A), shear wall pressure p_w (B), mobilized wall friction coefficient $\mu = p_w/p_h$ (C) and mobilized wall friction angle $\varphi_w = arc(tan\mu)$ (D) against filling/emptying time t for load cells located along silo height: C6 (a), C7 (b) and C8 (c) of Fig. 2 (— - wheat height H_m in [%]).

wall pressure's increase due to emptying was about 40–60% for the cells C1–C6, 30% for C7 and 10% for the cell C8 and shear wall pressure's growth was about 30–45%, 25% and 5%, respectively. The average increase of wall pressures along the silo circumference was 50% for the horizontal pressure and 35% for the frictional traction during emptying (Fig. 10b). The maximum differences between the highest and lowest horizontal/shear wall pressures along the silo circumference were about 15%/30% after filling and 20%/22% during emptying (Fig. 10b). The measured horizontal wall pressure and frictional traction during filling corresponded well to EC1 but during emptying the horizontal pressures were smaller by 10–25% in the lower silo region (C1–C6) and by 30–50% in the mid-region (C7–C8). The frictional traction was smaller by 1–20% and 15–35%, respectively (Fig. 10). Note that according to EC1, the increase of wall pressures during discharge is

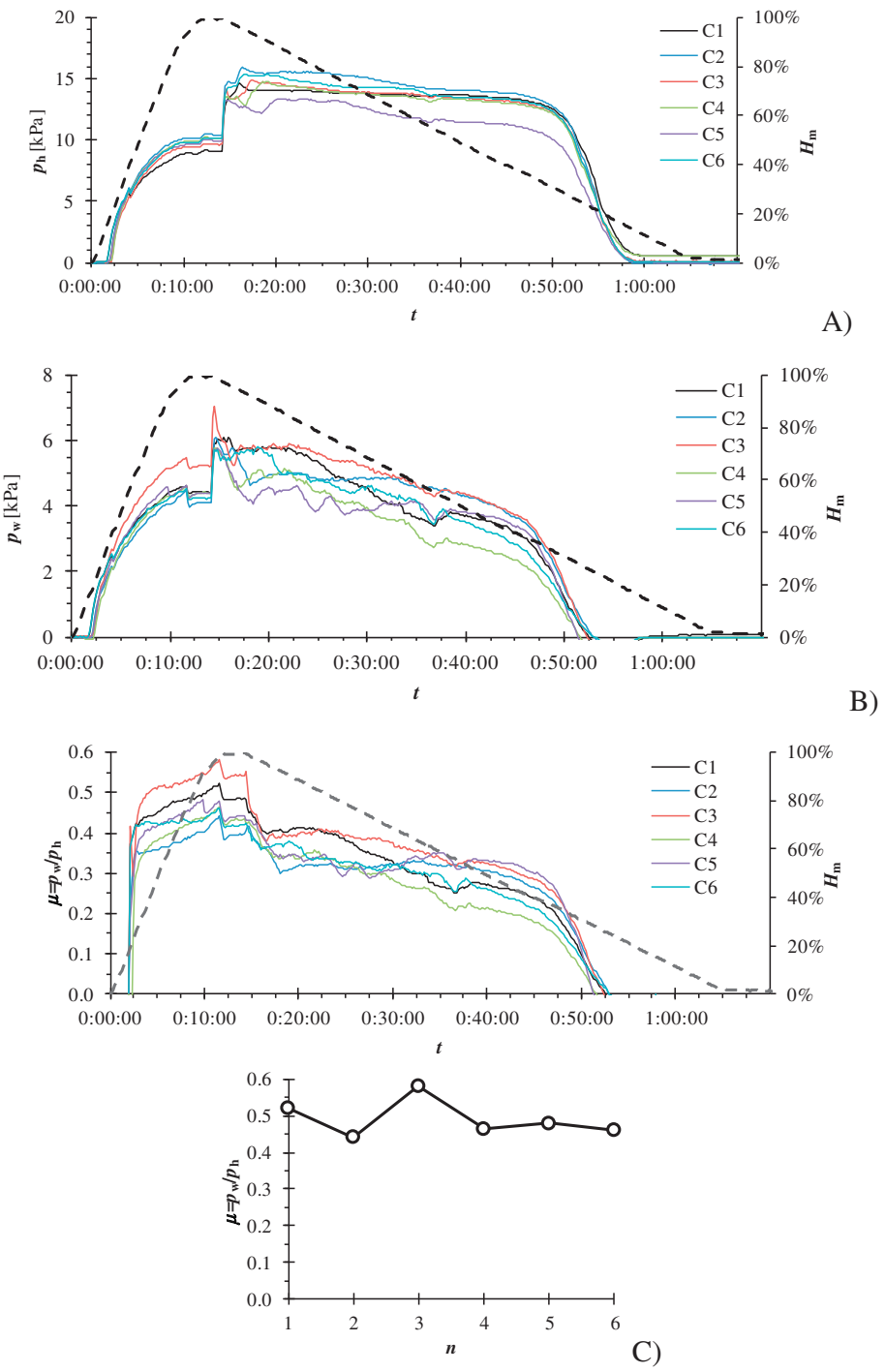

Fig. 9. Measured evolution of pressures for cells C1–C6 located along silo circumference (Fig. 2): A) horizontal wall pressure p_h and B) shear wall pressure p_w and C) mobilized wall friction coefficient $\mu = p_w/p_h$ against time t and its distribution along circumference for $t = 12$ min (–– wheat height H_m in [%], n – load cell number).

pronounced, i.e. 90% for the horizontal wall pressure and 40% for the wall frictional traction (since $C_h = 1.9$ and $C_w = 1.4$ in Eqs. (1) and (2)). EC1 does not take however a horizontal wall pressure variation into account along the circumference that occurred in our experiments (Fig. 10b).

The mobilized wall friction coefficient/angle (Figs. 8C, D, and 9C) reached the maximum value when the silo was pre-filled and was equal to $\mu/\varphi_w = 0.58/30°$ for the cell C3, $\mu/\varphi_w = 0.53/28°$ for C7 and $\mu/\varphi_w = 0.51/27°$ for C8. The average maximum wall friction coefficient/angle, calculated from all pressure cells (C1–C8), was $\mu/\varphi_w = 0.50/27°$ and was similar to the mean one assumed by Eurocode $\mu_{eff} = 0.54/\varphi_w = 28°$ (Eq. (4)). Next the mobilized wall friction coefficient/angle decreased during flow down to about 20° (slightly smaller than the measured repose angle of wheat - $\phi = 24°$). The wall friction coefficient/angle, which corresponded to the maximum wall pressure in the lower silo region (C6) (Fig. 8Aa) during emptying (for $t = 17$–18 min) was smaller, $\mu/\varphi_w = 0.37/20°$.

The measured silo results were repeatable. Fig. 11 presents the experimental maximum horizontal and shear wall pressures for load cells located along the silo circumference for 4 different tests. The

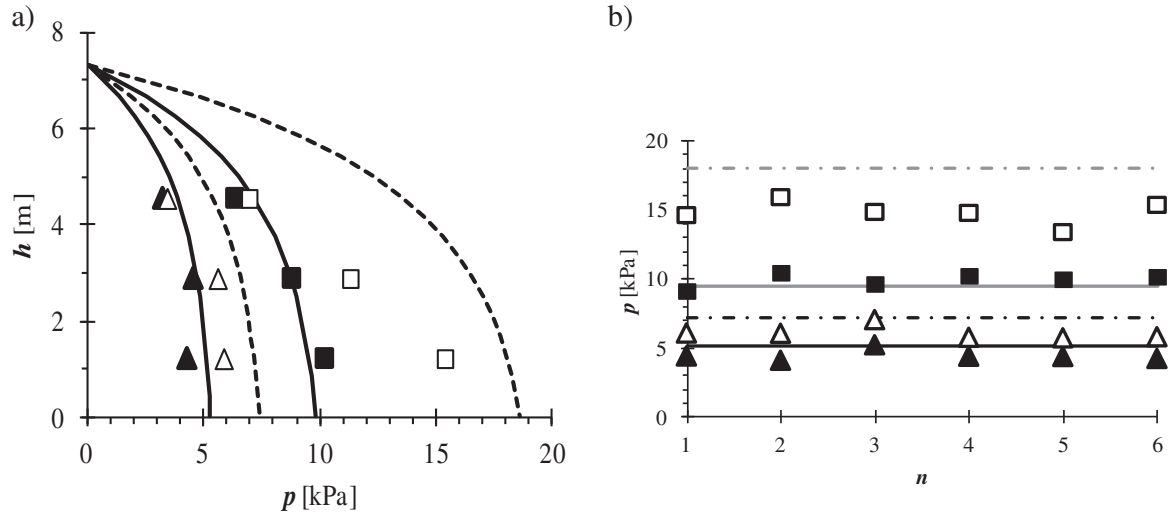

Fig. 10. Distribution of measured maximum horizontal and shear wall pressures p along silo height h (cells C6–C8) (a) and silo circumference (cells C1–C6) (b) with one centrally open outlet for filling and flow onset (one arbitrary test) as compared to EC 1 (— filling, - - - emptying, ▲ - frictional traction for filling p_{wf}, Δ - frictional traction for emptying p_{we}, ■ - horizontal pressure for filling p_{hf}, □ - horizontal pressure for emptying p_{he}, n - load cell number).

mean horizontal and shear wall pressures for filling and emptying in the lower silo region were: $p_{hf} = 10.1$ kPa, $p_{he} = 15.24$ kPa, $p_{wf} = 4.73$ kPa and $p_{we} = 6.19$ kPa with the standard deviation of 0.87, 0.83, 0.49 and 0.37, respectively.

The evolution of the measured 4 vertical reaction forces during silo filling and emptying under the supporting frame columns (F1–F4, Fig. 2) and 6 vertical reaction forces under silo columns (F11–F16, Fig. 2) is presented in Fig. 12A, whereas Fig. 12B shows their distribution along the silo circumference (F11–F16, Fig. 2). The results indicate that 60% (during filling) and 65% (during emptying) of the total solid weight was carried by silo wall and the rest was carried by the silo bottom. The vertical reaction forces in columns were similar; the difference was of the order of 10–15% in silo columns and about 5% in supporting frame columns, i.e. slightly smaller than the maximum local shear wall pressure changes along the circumference (20–30%, Fig. 10b). It was also observed that the reaction forces in 6 silo columns (Fig. 12A) were slightly

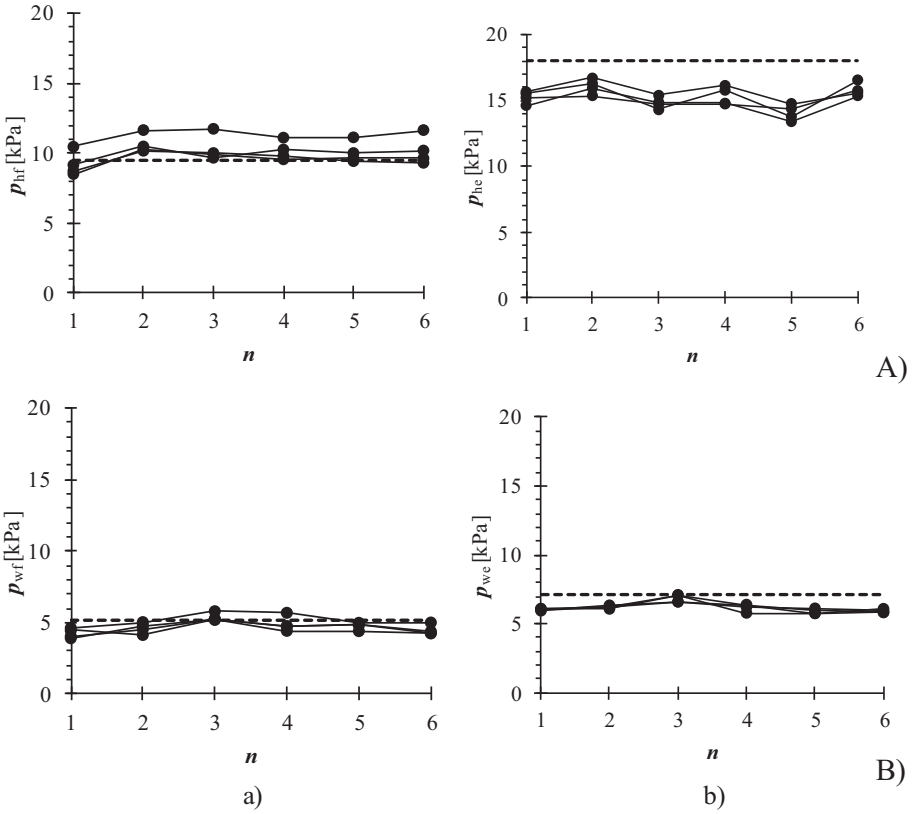

Fig. 11. Experimental maximum wall pressures for cells located along silo circumference for 4 tests with one centrally located outlet: A) horizontal wall pressure p_h, B) shear wall pressure p_w, a) filling and b) flow onset (n – number of pressure cell along silo circumference, —— - EC1).

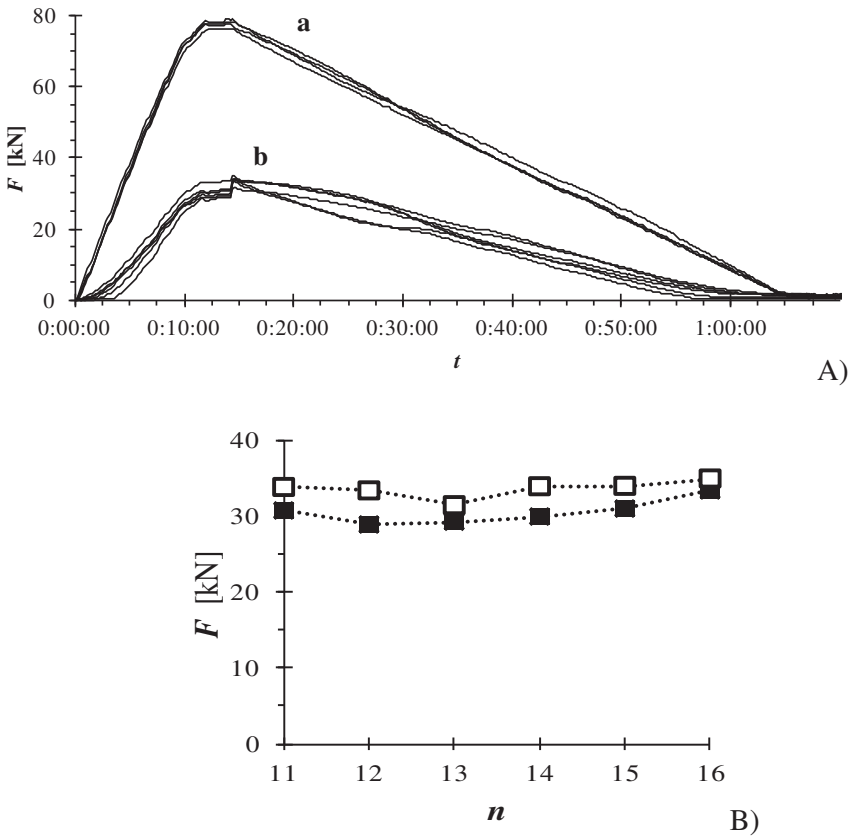

Fig. 12. Vertical reaction forces *F* during silo filling and emptying with one centrally open outlet: A) evolution in supporting frame columns (F1–F4, Fig. 2) (a) and in silo columns (F11-F16, Fig. 2) (b) and B) distribution in silo columns along circumference during filling (■) and emptying (□) (*n*- force transducer number).

influenced by their length, i.e. the load transfer started later in columns which were shorter by 1–2 mm that resulted in smaller reaction forces. The increase of vertical forces at the flow onset was relatively uniform (Fig. 12B). The mean increase was about 10% (Fig. 12B), i.e. smaller on average than the shear wall pressure increase (5–35%, Fig. 10a) along the silo height. The measured maximum compressive silo column forces, $N_{f,exp} = 33.5$ kN and $N_{e,exp} = 35$ kN, were lower by 20% during filling and by 35% during emptying than the values estimated by EC1: $N_f = 39.3$ kN (filling) and $N_e = 55.1$ kN (emptying).

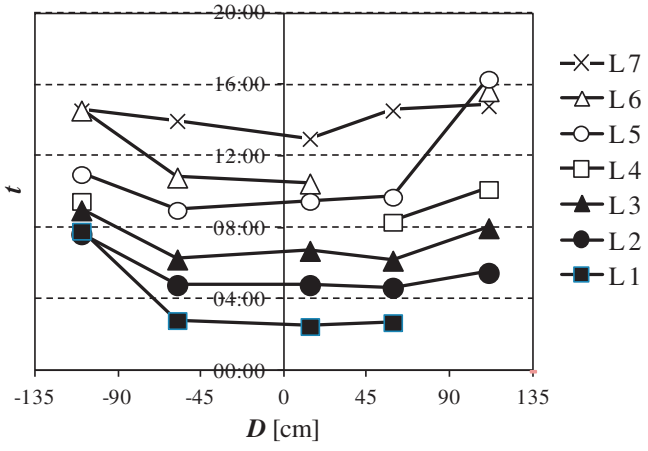

Fig. 13. Experimental results for corrugated silo with 5 open outlets: emptying times for markers located at different levels in cross-section D-H-I-F-B of Fig. 7a from one arbitrary test (L1–L7 - initial markers positions starting from silo bottom every 1 m), *D* - silo diameter, *t* - emptying time.

4.2. Wheat flow for all 5 open outlets '1-'5'

When all 5 bottom outlets were opened at the same time, the discharge flow rate was the highest (160 t/h). In this case almost all markers came out in a mass flow order, i.e. lines in Fig. 13 were almost horizontal and markers located at the lowest silo level came out as first ones.

The evolution of horizontal and shear wall pressures and mobilized wall friction coefficient/angle for load cells located along the silo height (load cells C6–C8) during silo filling and emptying for one arbitrary test and for load cells located along the silo circumference (load cells C1–C6) is demonstrated in Figs. 14 and 15. The distribution of the maximum wall normal and shear stresses measured during filling and emptying beginning along both the silo height and silo circumference is shown in Fig. 16 together with EC1 outcomes.

As compared to silo tests with one centrally open outlet, a stronger increase of wall pressures at the emptying beginning was registered, especially in the lower silo region wherein mass flow was created (Fig. 16). The increase of the horizontal wall pressure was 70–125% in the lower silo part (cells C1–C6) and 15%–50% at the silo mid-part (cells C7 and C8). The corresponding increase of the shear wall pressure was 45%–80% and 5–30%. The maximum horizontal and shear wall pressures for filling and emptying in the lower silo region were: $p_{hf} = 9.7$ kPa, $p_{he} = 18.3$ kPa, $p_{wf} = 4.9$ kPa and $p_{we} = 7.1$ kPa. The maximum mobilized wall friction coefficient (Fig. 15C) changed during flow from $\mu = 0.55$ ($\varphi_w = 29°$) after filling down to about $\mu \approx 0.45$ ($\varphi_w = 23.8°$) during flow. The wall friction coefficient/angle which corresponded to the maximum horizontal wall pressure in the lower silo part (C2) during emptying (for $t = 1{:}40$ h, Fig. 15B) was lower - $\mu/\varphi_w = 0.36/20°$.

Comparing with EC1, the measured maximum horizontal/shear wall pressures were lower by 0–15%/5–30% during filling and by 0–15%/1–

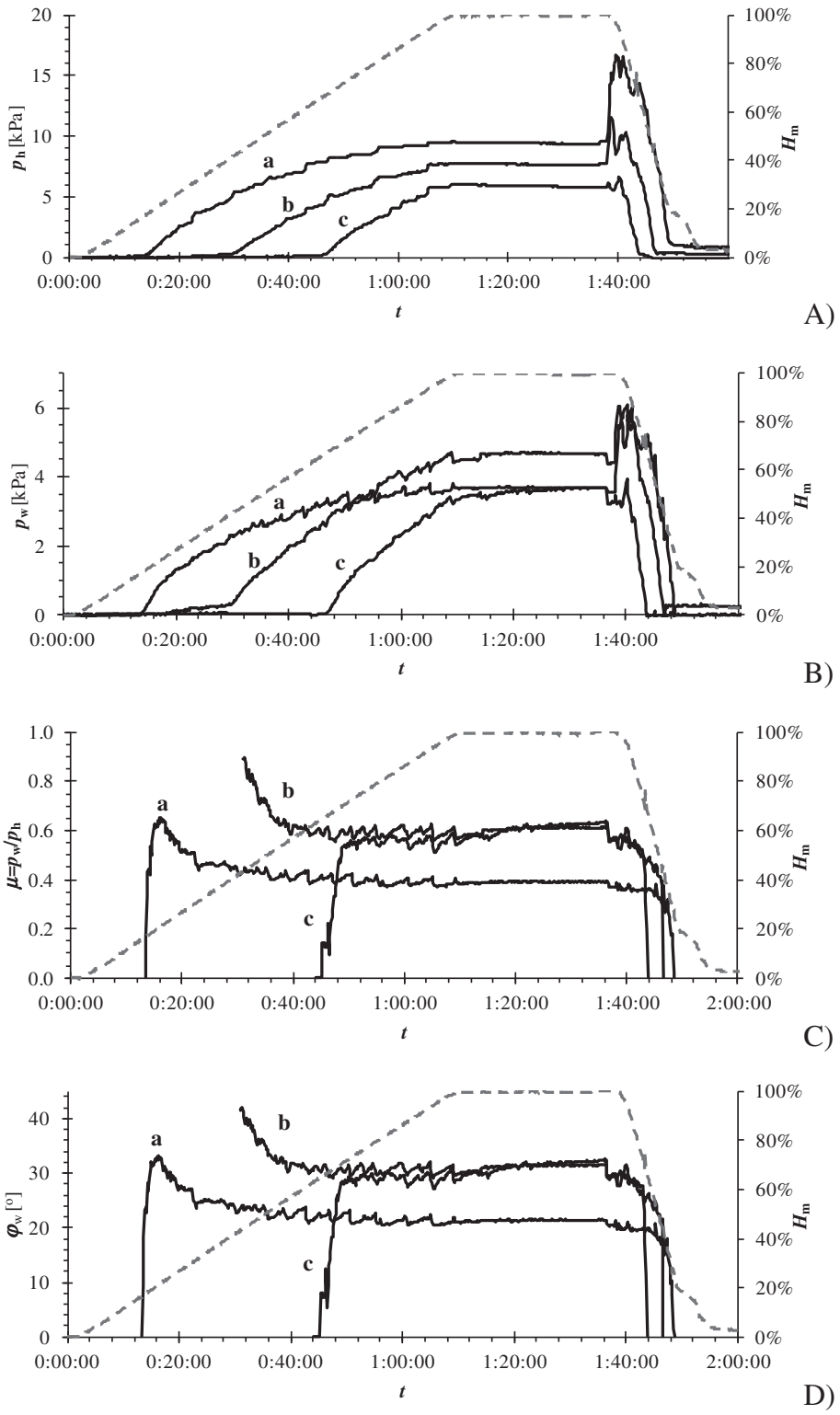

Fig. 14. Measurements from one arbitrary test with 5 open outlets: evolution of horizontal wall pressure p_h (A), shear wall pressure p_w (B), wall friction coefficient $\mu = p_w/p_h$ (C) and mobilized wall friction angle $\varphi_w = arc(tan\mu)$ (D) against time t for pressure cells located along height: C6 (a), C7 (b) and C8 (c) of Fig. 2a: (—— wheat height H_m in [%]).

15% during emptying in the lower silo region (Fig. 16). The maximum horizontal/shear wall pressure change around the circumference was 20%/35% (filling) and 17%/15% (emptying) (Fig. 16B) and was similar as in the case of one centrally open outlet (15%/30% (filling) and 20%/22% (emptying)).

The vertical reaction forces in silo columns differed by 15% for filling and by 25% for emptying. At the onset of mass flow the growth of vertical reaction forces in silo columns was about 5–35% (Fig. 17). The smallest increase was in the columns '13' and '16' located at the smallest distance from existing outlets (Fig. 2). The measured maximum vertical

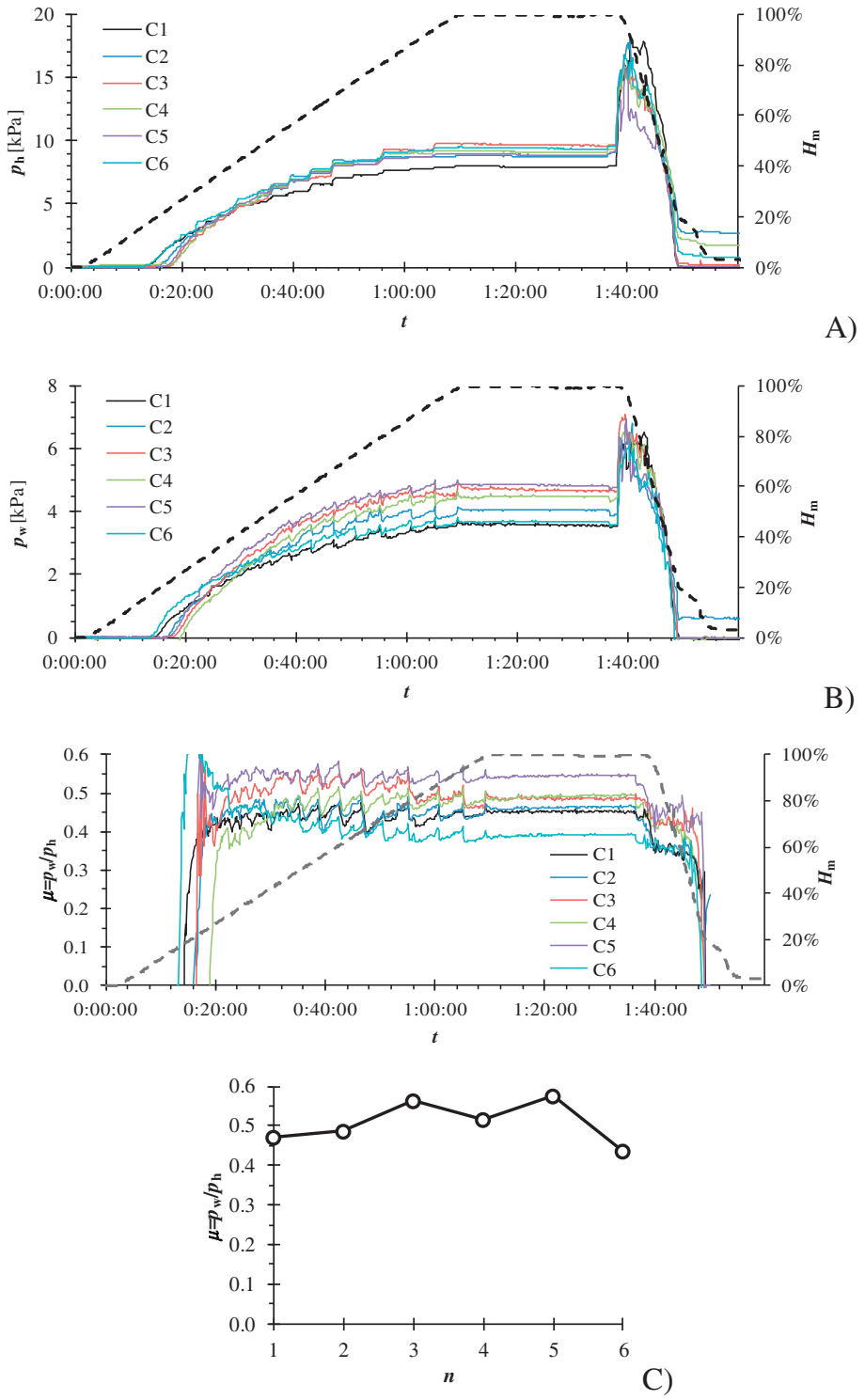

Fig. 15. Measured evolution of pressures in silo with 5 open outlets for cells located along silo circumference (Fig. 2): A) horizontal wall pressure p_h and B) shear wall pressure p_w, C) mobilized wall friction coefficient $\mu = p_w/p_h$ against time t and its distribution along circumference for $t = 36$ min (—— wheat height H_m in [%], n - load cell number).

force in silo columns (33 kN during filling and 40 kN during emptying) was smaller by 15% (filling) and by 30% (emptying) than this by EC1: $N_f = 39.3$ kN (filling) and $N_e = 55.1$ kN (emptying).

4.3. Wheat flow with one open non-symmetric outlet

One arbitrary non-axisymmetric open outlet ('2', '3' or '4') caused obviously non-symmetric flow, wherein wheat moved in funnel flow along one silo part only (Fig. 18), i.e. the markers located in the line 'B' (close to the silo wall) came out later than markers located on the opposite silo side. The effective flow transition point varied around silo circumference. In the lower silo region only, a clear narrow flow channel existed with the diameter of about 0.7–1.5 m. This diameter increased in the upper silo region up to D. This outcome is in contrast to EC1 for a large outlet eccentricity (Section 3.2) which assumes eccentric parallel pipe flow with a similar flowing channel diameter along the entire silo height

The evolution of the horizontal and shear wall pressures and mobilized wall friction coefficient/angle for load cells located along the silo

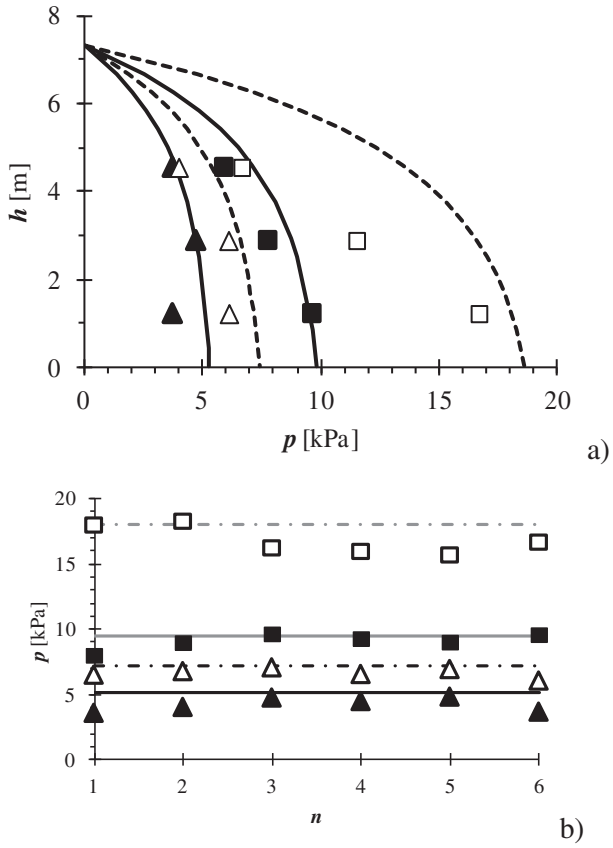

Fig. 16. Distribution of measured maximum normal and shear wall pressures p along silo height h (cells C6-C8) (a) and silo circumference (cells C1-C6 of Fig. 2) (b) with 5 open outlets for filling and flow onset (one arbitrary test) as compared to EC 1 (— filling, - - - emptying, ▲ - frictional traction for filling p_{wf}, Δ - frictional traction for emptying p_{we}, ■ - horizontal pressure for filling p_{hf}, □ - horizontal pressure for emptying p_{he}, n - cell number).

height (load cells C6–C8) during silo filling and emptying for one arbitrary tests is presented in Fig. 19 (with the open outlet '3'). The distribution of the maximum horizontal and shear wall pressures measured during filling and emptying is presented in Fig. 20 along the silo height and in Fig. 21 along the silo circumference when one different outlet was solely opened. The measured vertical reaction forces in silo columns are shown in Fig. 22.

At the flow onset, both the horizontal and shear wall pressures increased in regions beyond the narrow flow channel and decreased in the lower silo region close to the open outlet (Figs. 19-21). The horizontal

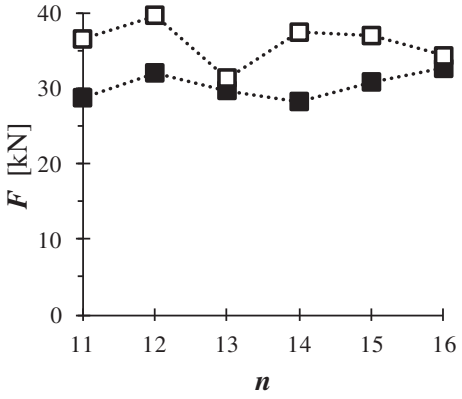

Fig. 17. Measured maximum vertical forces F in columns '11'–16' of silo with 5 open outlets during: ■ - filling and □ - emptying '5' (n - column load cell number).

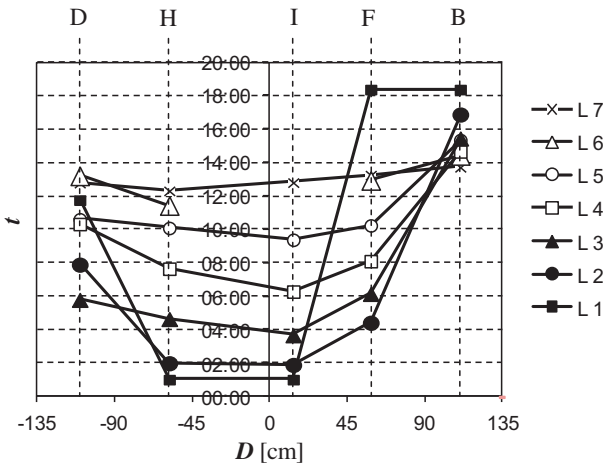

Fig. 18. Experimental results for corrugated silo with 1 open outlet '3': emptying times for markers located at different levels in cross-section D-H-I-F-B of Fig. 7a from one arbitrary test (L1–L7 - initial markers positions starting from the silo bottom every 1 m), D - silo diameter, t - emptying time.

and shear wall pressure's growth, measured along the silo circumference (at $h = 1.22$ m) during flow far beyond the narrow flow channel edge, was about 30–55% and 10–40%, whereas measured at the flow channel decreased by 60–65% and by 65–67%, respectively (load cells C2 and C5, Fig. 21). In the higher silo region (load cell C7 for $h = 2.90$ m and load cell C8 for $h = 4.57$ m), both the horizontal and shear pressures increased by 35–73% and 16–47%, independently of the outlet location (Fig. 20) due to a wide flow channel with a diameter close to D. In the lower silo region (cells '1'–'6') the maximum horizontal wall pressure was smaller by 20% than those for 5 open outlets, whereas in higher regions was larger by 25% (cell '7') and 60% (cell '8'). The maximum shear pressure was similar in lower regions and larger by 10% and 25%, respectively (Figs. 20 and 21).

The maximum mobilized wall friction coefficient changed during flow on average from $\mu = 0.55$ ($\varphi_w = 29°$) down to $\mu = 0.45$ ($\varphi_w = 24°$).

According to EC1 for the flow channel radius $r_c = 0.4R = 0.53$ m (Fig. 6), the horizontal wall pressure at the flow channel should decrease and at the flow channel edge should increase by the same value of 60%. For the other flow channel radii, the change should be 40% for $r_c = 0.6R = 0.8$ m and 75% for $r_c = 0.25R = 0.33$ m (Fig. 6). Thus the best agreement between the experimental outcomes in the lower silo region and EC1 was for $r_c = 0.4R = 0.53$ m (the measured values were smaller by 0–10% for horizontal pressures and by 20–25% for shear pressures (Fig. 21b and d)). EC1 indicates no wall pressure changes on the opposite side of the open outlet that is inconsistent with experimental results wherein the wall pressure's growth was measured of about 30–55% for horizontal pressures and 10–40% for shear ones (Fig. 21).

At the flow onset, the vertical reaction forces in silo columns near the open outlet increased by 25–30% while these forces in silo columns on the opposite side remained almost unchanged (Fig. 22). The vertical reaction forces' increase in columns located close to a flow channel was smaller by 20% than in columns located at a flow channel edge.

4.4. Wall pressures on flat wall segment

Fig. 23 presents the evolution of the measured horizontal and shear wall pressures and wall friction coefficient for 5 simultaneously open outlets '1'–'5' (mass flow). The wall pressures were measured by the load cell C9 located in the inspection opening door.

The maximum horizontal wall pressure at the flow onset was 17.1 kPa (Fig. 23). As compared to the horizontal wall pressure measured by the load cell 'C1' in the corrugated wall, located by 0.83 m higher than the load cell C9, the horizontal pressure's increase during

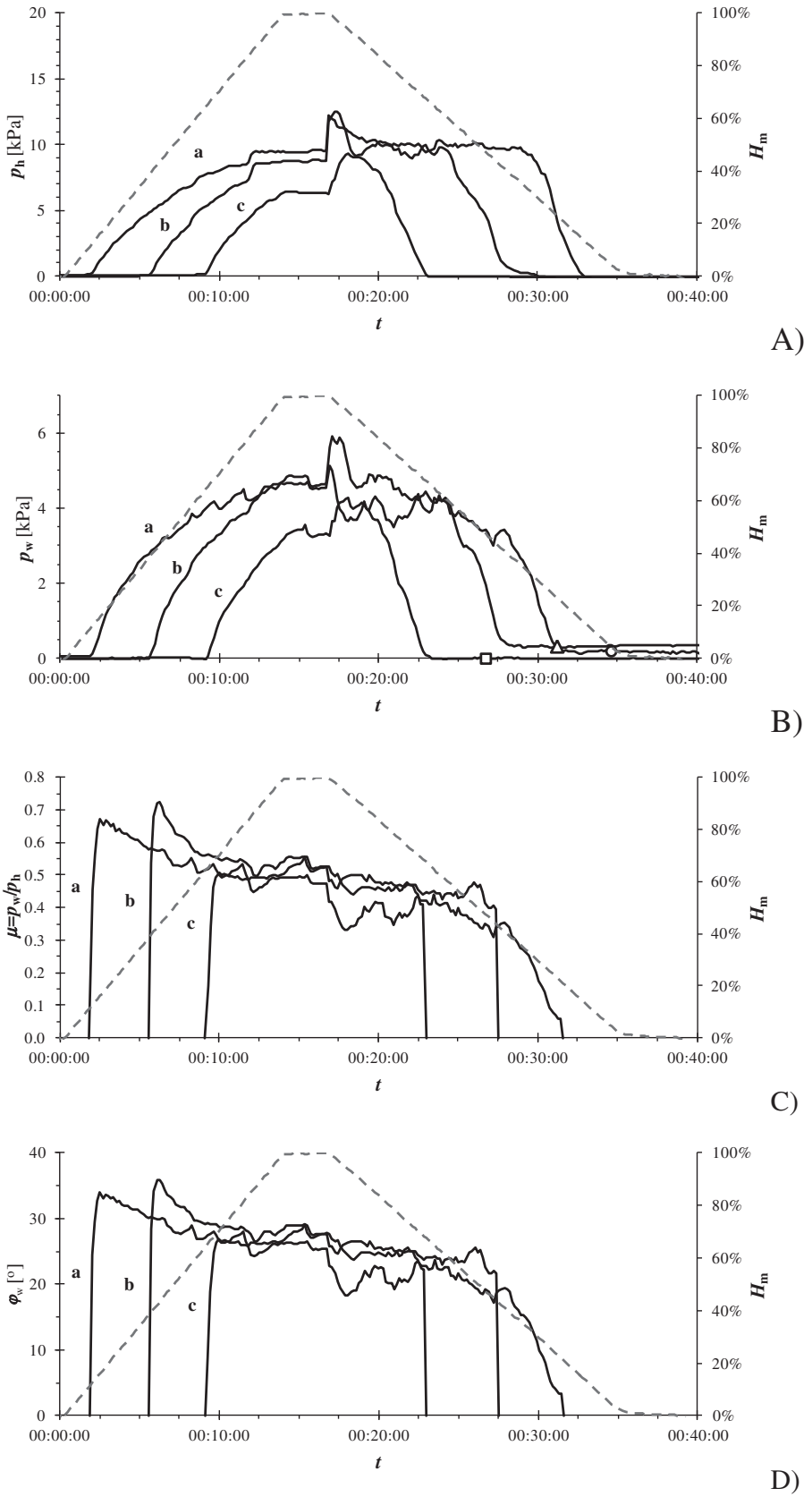

Fig. 19. Measurements from one arbitrary test with one open outlet '3': evolution of horizontal wall pressure p_h (A), shear wall pressure p_w (B), mobilized wall friction coefficient $\mu = p_w/p_h$ (C) and mobilized wall friction angle $\varphi_w = arc(tan\mu)$ (D) against time t for pressure cells located along height: C6 (a), C7 (b), C8 (c) of Fig. 2 (— - wheat height H_m in [%]).

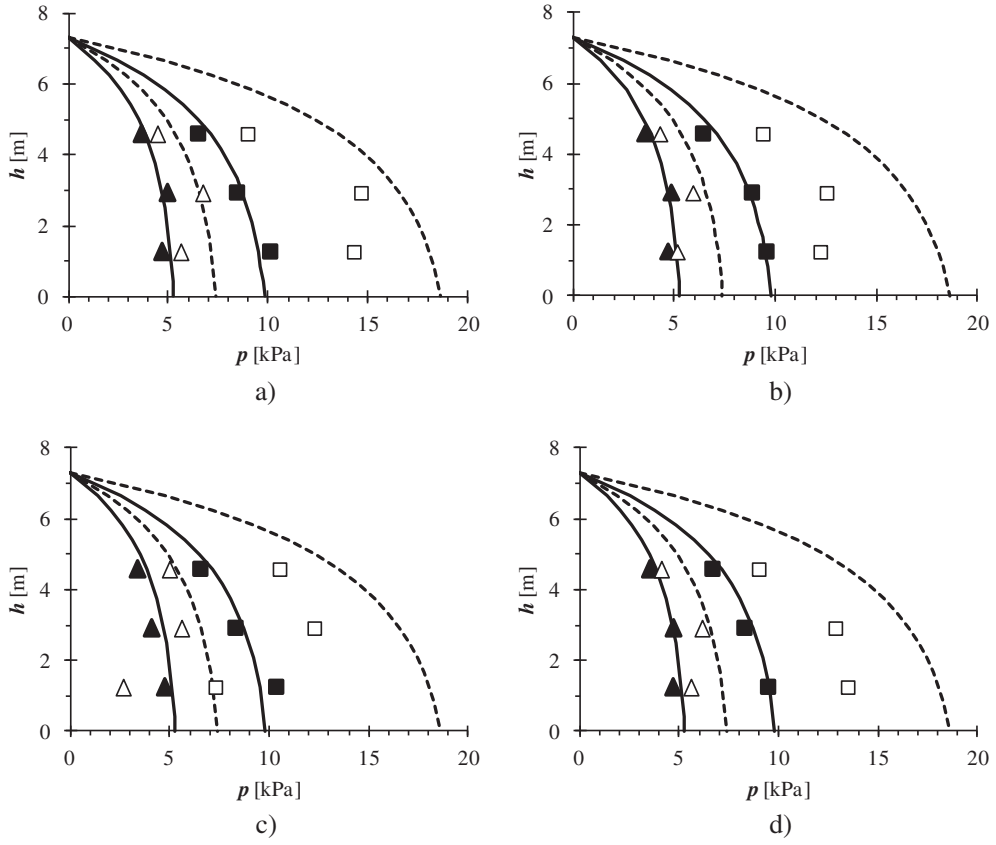

Fig. 20. Distribution of measured maximum horizontal and shear wall pressures (cells C6–C8) along silo height h with 1 non-centrally open outlet after filling and at flow onset for different open outlets versus EC1: a) open outlet '2', b) open outlet '3', c) open outlet '4' and d) open outlet '5' (— filling, - - - - emptying, ▲ - frictional traction for filling p_{wf}, Δ - frictional traction for emptying p_{we}, ■ - horizontal pressure for filling p_{hf}, □ - horizontal pressure for emptying p_{he}).

emptying was smaller by 30%. The maximum wall shear pressure at the flow onset was 4.6 kPa (Fig. 23). As compared to the shear wall pressure exerted on the corrugated wall, the shear pressure's increase was smaller by 20%. The maximum mobilized wall friction coefficient measured with the load cell (C9) located in the inspection opening was about $\mu = 0.2$ ($\varphi_w = 12°$) during filling and $\mu = 0.3$ ($\varphi_w = 17°$) during emptying. Thus it was significantly smaller as compared to the corrugated wall due to a flat measuring surface of the pressure cell. Note that the maximum value of μ was reached during flow and not during filling (as for corrugated walls).

5. Conclusions

The main outcomes from our experiments in a full-scale steel cylindrical silo with corrugated walls and open-sectional thin-walled column profiles containing cohesionless wheat with the mean initial volumetric weight of 7.75 kN/m^3 are the following:

- The horizontal and shear wall pressures always increased after outlet opening. The largest wall pressures obviously occurred in the lower silo part during mass flow (higher by 70–120% for horizontal pressures and by 45–80% for shear pressures than during filling). In the mid- and upper silo region, the highest horizontal and shear wall pressures appeared during eccentric flow (higher by 35–75% for the horizontal and 15–45% for the shear pressure than during filling). The measured maximum horizontal wall pressures in the lower region were smaller than those by EC1 (Eqs. (1)–(4)) by 10–25% for mixed flow, by 20–35% for eccentric flow and were similar for mass flow. The measured maximum shear wall pressures was smaller than 1–20%, 3–35% and 1%, respectively. The distribution of horizontal wall pressures during flow was almost linear in contrast to the Janssen's theory. The EC1 procedures provide wall pressures on a safe side by taking also into account the fact that the experimental silo was relatively small and normalized wall pressures in larger silos are expected to be lower due to a higher pressure level.

- During flow with a large outlet eccentricity, partially eccentric mixed flow occurred in contrast to EC1 which assumed eccentric parallel pipe flow. During this flow, both the horizontal and shear wall pressures increased in regions far beyond the flow channel and decreased in the lower silo region close to the open outlet. As compared do EC1 with $r_c = 0.4R$ (Figs. 5 and 6), the measured wall pressures were greater by 30–55% (horizontal pressures) and 10–40% (shear pressure) on the opposite side of the single open outlet (EC1 assumes no wall pressure changes) and by 0–10% (horizontal pressures) and 20–25% (shear pressures) too small in the region close to a single open outlet.

- The maximum mobilized wall friction angle was always the highest after filling. Afterwards it reduced during flow. The average maximum wall friction angle at the silo bottom was for filling $\varphi_w = 27°–29°$ ($\mu = 0.50–0.55$). It was in agreement with the values proposed by EC1: $\varphi_w = 25°–32°$ ($\mu = 0.47–0.62$). However the value corresponding to the maximum horizontal wall pressure ($\varphi_w = 20–25°$) was smaller than the EC1-values. The measured minimum wall friction angle during flow was about 20° and approximately corresponded to the angle of repose of wheat.

- In spite of symmetric filling, the flow was always non-symmetric. The horizontal/shear pressure difference along the silo circumference was about 20%/35% and 17%/15% during mass flow (filling

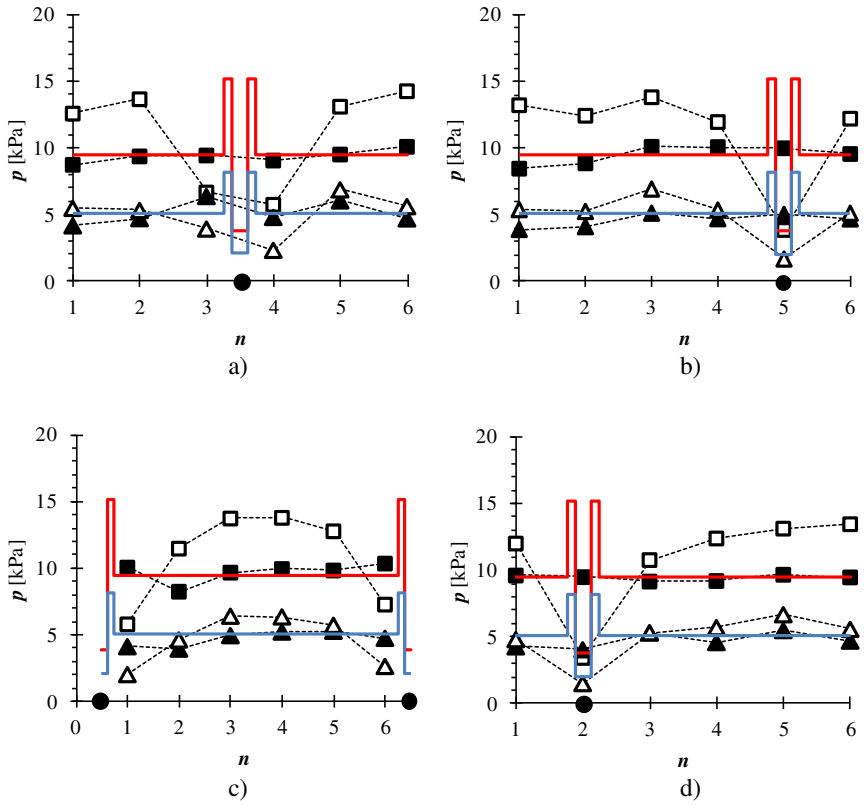

Fig. 21. Distribution of measured maximum horizontal and shear wall pressures (cells C1–C6) from tests with non-symmetric open outlets (marked by circle) after filling and during flow along silo circumference (▲ - frictional traction for filling p_{wf}, Δ - frictional traction for emptying p_{we}, ■ - horizontal pressure for filling p_{hf}, □ - horizontal pressure for emptying p_{he}, n - load cell number along circumference): a) open outlet '2', b) open outlet '3', c) open outlet '4' and d) open outlet '5', EC1 (— normal pressure, — shear pressure) for $r_c = 0.53$ m.

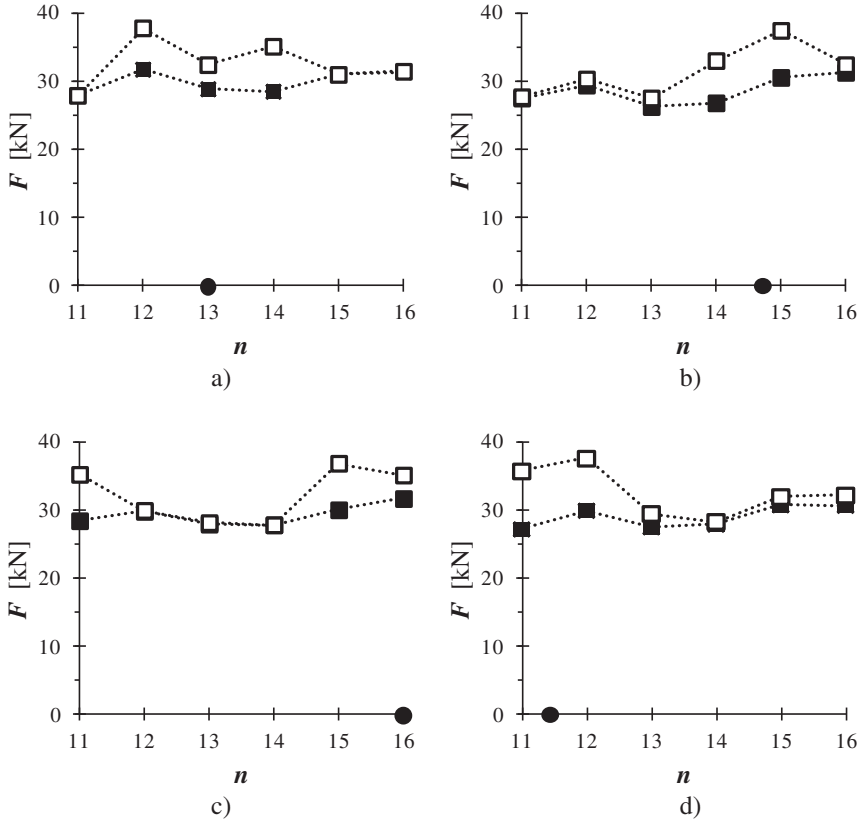

Fig. 22. Experimental vertical reaction forces in columns F11–F16 after filling (■) and at flow onset (□) with 1 non-centrally located opening marked by circle (•): a) open outlet '2', b) open outlet '3', c) open outlet '4' and d) open outlet '5' (n - force transducer number).

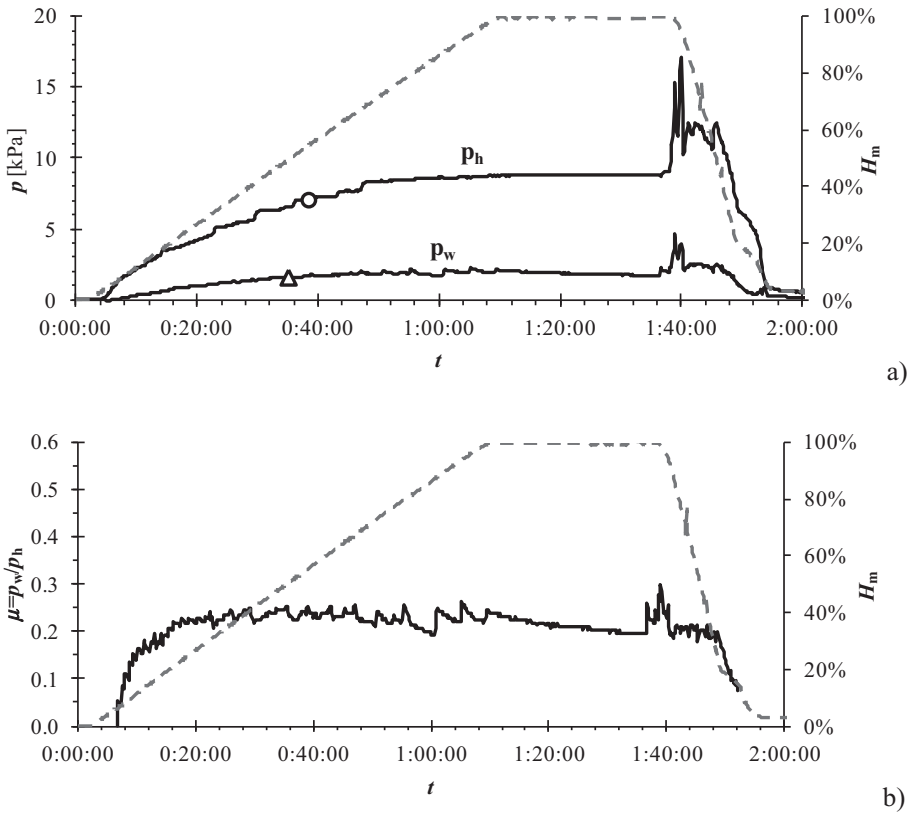

Fig. 23. Measured evolution of horizontal wall pressure p_h and shear wall pressure p_w (a) and wall friction coefficient μ on flat wall segment in inspection door (load cell C9) from one arbitrary test for open outlets '1'–'5' (— - material height H_m [%])

and emptying), 15%/30% and 20%/22% during concentric mixed mass-funnel flow (filling and emptying). The resultant column vertical force difference along the silo circumference was 25% during mass flow, 10% during concentric mixed flow and 30–35% during eccentric flow. EC1 takes into account this non-uniformity in all cases but it may be ignored in silos of the Reliability Class 1 because other coefficients and procedures are on the safe side.

Acknowledgement

We acknowledge the support from the Grant WND-POIG.01.03.01-00-099/12-01 financed by the Polish National Centre for Science and Development (NCBiR).

The help of K. Rejowski in the experiments' performance is acknowledged.

References

[1] A.W. Jenike, Storage and flow bulk of solids, Eng. Exp. Station Bull. No 123, University Utah, 1964.
[2] J. Schwedes, Fließverhalten von Schüttgütern in Bunkern, Verlag Chemie, Weinheim/Bergstraße, 1970.
[3] N. Fayed, L. Otten, Handbook of Powder Science and Technology, Chapmann and Hall, 1984.
[4] S.S. Safarian, E.C. Harris, Design and Construction of Silos and Bunkers, Van Nostrand Reinhold Company, 1985.
[5] E. Hampe, Silos, VEB Verlag für Bauwerke, Berlin, 1987.
[6] C.J. Brown, J. Nielsen, Silos – Fundamentals of Theory, Behaviour and Design, E and FN Spon, 1998.
[7] M. Rotter, Guide for the Economic Design of Circular Metal Silos, Spon Press, 2001.
[8] J. Ravenet, Silo problems, Bulk Solids Handl. 1 (4) (1981) 667–679.
[9] J.W. Carson, Silo failures: case histories and lessons learned, Proc. 3rd Israeli Conf. for Conveying and Handling of Particulate Solids, Dead Sea, Israel, 1, 2000, pp. 1–4.
[10] A. Dogangun, Z. Karaca, A. Durmus, M. Halil Sezen, Cause of damage and failures in silo structures, J. Perform. Constr. Facil. ASCE 23 (2) (2009) 65–71.
[11] J. Tejchman, Confined Granular Flow in Silos – Experiments and Numerical Investigations, Springer, Berlin-Heidelberg, 2013.
[12] J. Tejchman, FE modeling of shear localization in granular bodies with micro-polar hypoplasticity, Springer Series in Geomechanics and Geoengineering, Berlin-Heidelberg, 2008.
[13] P. Iwicki, M. Wójcik, J. Tejchman, Failure of cylindrical steel silos composed of corrugated sheets and columns and repair methods using a sensitivity analysis, Eng. Fail. Anal. 18 (2011) 2064–2083.
[14] P. Iwicki, M. Sondej, J. Tejchman, Application of linear buckling sensitivity analysis to economic design of cylindrical steel silos composed of corrugated sheets and columns, Eng. Fail. Anal. 70 (2016) 105–121.
[15] M. Wójcik, J. Tejchman, Simulation of buckling process of cylindrical metal silos with flat sheets containing bulk solids, Thin-Walled Struct. 93 (2015) 122–136.
[16] N. Kuczyńska, M. Wójcik, J. Tejchman, Effect of bulk solid on strength of cylindrical corrugated silos during filling, J. Constr. Steel Res. 115 (2015) 1–17.
[17] V. Askegaard, J. Munch-Andersen, Results from tests with normal and shear stress cells in a medium-scale model silo, Powder Technol. 44 (1985) 151–157.
[18] J.Y. Ooi, L. Pham, J.M. Rotter, Systematic and random features of measured pressures on full-scale silo walls, Eng. Struct. 12 (1990) 74–87.
[19] C.J. Brown, E.H. Lahlouh, J.M. Rotter, Experiments on a square platform steel silo, Chem. Eng. Sci. 55 (2000) 4399–4413.
[20] Z. Zhong, J.Y. Ooi, J.M. Rotter, The sensitivity of silo flow and wall stresses to filling method, Eng. Struct. 23 (2001) 756–767.
[21] F. Ayuga, M. Guaita, P. Aguado, Static and dynamic silo loads using finite element models, J. Agric. Eng. Res. 78 (3) (2001) 299–308.
[22] J.M. Rotter, C.J. Brown, E.H. Lahlouh, Patterns of wall pressure on filling a square planform steel silo, Eng. Struct. 24 (2002) 135–150.
[23] M. Molenda, M.D. Montross, J. Horabik, Non-axial stress state in a model silo generated by eccentric filling and internal inserts, Part. Part. Syst. Charact. 24 (2007) 291–295.
[24] J.F. Chen, J.M. Rotter, J.Y. Ooi, Z. Zhong, Correlation between the flow pattern and wall pressures in a full scale experimental silo, Eng. Struct. 29 (2007) 2308–2320.
[25] J. Härtl, J.Y. Ooi, J.M. Rotter, M. Wójcik, S. Ding, G.G. Enstad, The influence of a cone-in-cone insert on flow pattern and wall pressure in a full-scale silo, Chem. Eng. Res. Des. 86 (2008) 370–378.
[26] A. Ramirez, J. Nielsen, F. Ayuga, Pressure measurements in steel silos with eccentric hoppers, Powder Technol. 201 (2010) 7–20.
[27] S. Ding, J.M. Rotter, J.Y. Ooi, G. Enstad, Development of normal pressure and frictional traction along the walls of a steep conical hopper during filling, Thin-Walled Struct. 49 (2011) 1246–1250.
[28] M. Wójcik, J. Tejchman, G.G. Enstad, Confined granular flow in silos with inserts - full-scale experiments, Powder Technol. 222 (2012) 15–36.
[29] A. Couto, A. Ruiz, L. Herráez, J. Moran, P.J. Aguado, Measuring pressures in a slender cylindrical silo for storing maize. Filling, static state and discharge with different

material flow rates and comparison with Eurocode 1 part 4, Comput. Electron. Agric. 96 (2013) 40–56.
[30] P. Iwicki, K. Rejowski, J. Tejchman, Stability of cylindrical steel silos composed of corrugated sheets and columns based on FE analyses versus Eurocode 3 approach, Eng. Fail. Anal. 57 (2015) 444–469.
[31] M. Sondej, P. Iwicki, J. Tejchman, M. Wójcik, Critical assessment of Eurocode approach to stability of metal cylindrical silos with corrugated walls and vertical stiffeners, Thin-Walled Struct. 95 (2015) 335–346.
[32] M. Sondej, P. Iwicki, M. Wójcik, J. Tejchman, Stability analyses of a cylindrical steel silo with corrugated sheets and columns, Steel Compos. Struct. 20 (1) (2016) 147–166.
[33] EN 1991-4, Eurocode 1: actions on structures. Part 4: silos and tanks, General Principles and Actions for the Structural Design of Tanks and Silos, 2006.
[34] M. Wójcik, J. Tejchman, Modeling of shear localization during confined granular flow in silos within non-local hypoplasticity, Powder Technol. 192 (2009) 298–310.
[35] A. Ramírez, J. Nielsen, F. Ayuga, On the use of plate-type normal pressure cells in silos: part 1: calibration and evaluation, Comput. Electron. Agric. 71 (1) (2010) 71–76.
[36] A. Ramírez, J. Nielsen, F. Ayuga, On the use of plate-type normal pressure cells in silos: part 2: validation for pressure measurements, Comput. Electron. Agric. 71 (1) (2010) 64–70.